



# Spatial distribution of vertical carbon fluxes on the Agulhas Bank and its possible implication for the benthic nepheloid layer

Nwabisa V. Malongweni<sup>a,\*</sup>, Emma Roche<sup>b</sup>, Michael J. Roberts<sup>a,c</sup>, Sarah L.C. Giering<sup>c</sup>

<sup>a</sup> Nelson Mandela University, Gqeberha, 6001, South Africa

<sup>b</sup> Department of Biological Sciences and Marine Research Institute, University of Cape Town, 7701, South Africa

<sup>c</sup> Ocean Biogeosciences, National Oceanography Centre, Southampton, United Kingdom

## ARTICLE INFO

Handling Editor: Prof. J. Aristegui

### Keywords:

Bottom turbidity  
BNL  
Shelf seas  
Agulhas Bank  
POC  
Biogenic silica  
Chlorophyll *a*  
Flux  
Export efficiency  
Transfer efficiency

## ABSTRACT

Vertical particle fluxes of particulate organic carbon (POC), chlorophyll *a* (Chl *a*) and biogenic silica (bSi) were measured on the productive shelf of southern Africa, the Agulhas Bank (AB), in March 2019. Sinking particulate material in the form of aggregates is hypothesized to form the benthic nepheloid layer (BNL) which is a turbid layer found near the seabed. This layer is known to affect the spawning success of squid as it is linked to high turbidity which reduces visibility during mating. To determine the distribution of fluxes and particle composition in the AB, we collected water samples below the surface mixed layer ('export') and near the seabed ('bottom') using a Marine Snow Catcher. POC export fluxes were significantly higher inshore than offshore (mean  $\pm$  SD:  $944.6 \pm 302.0$  &  $461.1 \pm 162.1$  mg POC  $m^{-2} d^{-1}$ , respectively). There was no significant difference in the cross-shelf distribution of Chl *a* and bSi export fluxes, however the inshore fluxes of Chl *a* and bSi were higher than offshore, suggesting a link between export fluxes and sinking organic matter derived from the more productive inshore surface waters. All bottom fluxes were significantly higher inshore, suggesting the contribution of sinking organic particles and resuspended bottom sediments to inshore fluxes. POC export efficiency (ratio of exported POC flux relative to net primary production (NPP)) was higher on the AB (range: 0.58–9.56) compared to the global shelf seas ratio of 0.18 and not related to NPP, suggesting an export of standing stock of carbon biomass, likely produced before the cruise. Transfer efficiency (i.e., the amount of exported flux that reaches the bottom) was also high (max: 0.99, 1.0 and 33.04 for POC, Chl *a* and bSi, respectively) but did not show a clear spatial pattern. We observed a significant positive correlation between bottom turbidity (a proxy for BNL presence) and export POC flux, suggesting the possibility that sinking organic matter is contributing to BNL formation on the AB.

## 1. Introduction

Shelf seas, typically 200 m or shallower, are the most productive regions of the global ocean supporting the world's major fisheries (Simpson and Sharples, 2012). Though shelf seas occupy about 7.6% of the world's ocean, their phytoplankton production is  $\sim 3 - 5$  times higher than the open ocean, supporting approximately 90% of the world's fish yield (Holt et al., 2017; Simpson and Sharples, 2012; Watson and Pauly, 2001). Factors such as coastal upwelling and riverine input contribute to the shelf's primary production through the introduction of nutrients into the system (Atkinson et al., 1984; Liu et al., 2000). Shelf seas play a major role in carbon cycling by trapping notable amounts of atmospheric CO<sub>2</sub> (0.33–0.36 Pg C yr<sup>-1</sup>) which is fixed and

transferred to the deep ocean via the continental shelf pump (Chen and Borges, 2009; Holt et al., 2017; Thomas et al., 2004). Additionally, shelf seas form an exchange barrier of materials between land and the deep ocean (de Haas et al., 2002; Holt et al., 2017; Simpson and Sharples, 2012).

The shelf on the southern coast of Africa – the Agulhas Bank (AB) – lies between 18°E – 29°E and 34.8°S – 36.9°S, extends to 200 m isobath and is about 116 000 km<sup>2</sup> (Boyd and Shillington, 1994; Hutchings, 1994). The Agulhas Bank is divided into three parts: the eastern Agulhas Bank (EAB), the central Agulhas Bank (CAB) and the western Agulhas Bank (WAB). Each has its own distinguishable oceanographic and circulation patterns. The EAB is influenced by the fast-flowing, warm western boundary Agulhas current (AC) along the south-east coast of

\* Corresponding author.

E-mail address: [malongwenin@gmail.com](mailto:malongwenin@gmail.com) (N.V. Malongweni).

<https://doi.org/10.1016/j.dsr2.2023.105334>

Received 28 June 2022; Received in revised form 5 September 2023; Accepted 19 September 2023

Available online 21 September 2023

0967-0645/© 2023 The Authors. Published by Elsevier Ltd. This is an open access article under the CC BY-NC-ND license (<http://creativecommons.org/licenses/by-nc-nd/4.0/>).

South Africa (SA) where shelf-edge upwelling is known to take place (Beal et al., 2011; Lutjeharms, 2006; Roberts and van den Berg, 2005), while the WAB (Cape Point to Cape Agulhas) is influenced by the cold Benguela current (Hutchings, 1994). There is also a periodic cool water feature (the ‘cold-ridge’ cell) between Mossel Bay and Cape St Francis which is associated with high primary production, hypothesized to be due to the introduction of cool nutrient-rich waters onto the shelf (Swart and Largier, 1987; Walker, 1986). All these characteristics make the Agulhas Bank a very complex system.

In terms of productivity, the Agulhas Bank recorded an average annual net primary productivity (NPP) of  $516 \text{ g C m}^{-2} \text{ yr}^{-1}$  over a 20-year period (1998–2018) (Mazwane et al., this issue). This is greater than the global shelf annual NPP averages of  $250\text{--}300 \text{ g C m}^{-2} \text{ yr}^{-1}$  (Boyd et al., 2014) and  $385 \text{ g C m}^{-2} \text{ yr}^{-1}$  (Longhurst et al., 1995). Due to its productivity, the Agulhas Bank provides a good habitat for spawning and is a nursery ground for commercial demersal and pelagic fish (Hutchings, 1994; Hutchings et al., 2002). For example, squid spawn inshore of the EAB, CAB and the west coast; then migrate in any direction to feed, and some may return inshore to complete their lifecycle (Lipiński et al., 2016). Enhanced primary production may lead to increased vertical transport of organic matter (OM) to the ocean interior (de Haas et al., 2002).

As organic matter sinks to the bottom of the water column, it is remineralized by microbes and/or consumed by zooplankton, resulting in a minute fraction of organic carbon reaching the seabed for burial in the global ocean i.e.,  $\sim 0.2\text{--}0.4 \text{ Pg C y}^{-1}$  (Middelburg, 2019). However, the shelf sea sediments tend to receive more organic matter when compared to the open ocean due to their shallow depth (Middelburg, 2019). Areas of high primary productivity, coupled with low remineralization rates, may result in a higher export flux of organic carbon below the upper mixed layer. For example, Lutz et al. (2002) reported high vertical fluxes of carbon due to primary production in the Arabian Sea, Panama Basin, subarctic Pacific and Southern Ocean/Atlantic sector and shallow ocean. It is unclear how vertical carbon fluxes are distributed on the Agulhas Bank. Consequently, the main goal of this study was to investigate the distribution of vertical carbon fluxes and its implications for the benthic nepheloid layer (BNL) formation in this region.

BNLs may form when hydrodynamic forces produce strong currents which can resuspend bottom sediments (Ewing and Thorndike, 1965; Gardner et al., 2018; Hollister and McCave, 1984; McCave, 1983). BNLs can also form when particulate matter sinks from the ocean surface and accumulates at depth (Faugères and Mulder, 2011; Kalle, 1937; Karp-Boss et al., 2004; McCave, 1983; McCave and Hall, 2002). A BNL is usually found a few meters above the seabed with increased suspended particulate matter (SPM) compared to surrounding waters (McCave, 1983; Pak and Zaneveld, 1977; Townsend et al., 1992). The suspended particulate matter in the BNL may remain suspended for various periods of time due to turbulent mixing (Faugères and Mulder, 2011; Shideler, 1981) caused by internal waves or swells and disappear when the conditions are favourable for particles to re-settle (Roberts and Sauer, 1994). On the Agulhas Bank, the events of turbid bottom water or BNLs have been recorded periodically inshore from the 100 m isobath with the most intense events observed within embayments or capes and it has been suggested that they may disturb the spawning of adult South African ‘‘chokka’’ squid due to reduced visibility (Dorfler, 2002; Roberts and Sauer, 1994; Zoutendyk, 1972). However, it is uncertain what forms these high turbidity events on the AB which can lead to the presence of a BNL.

The purpose of this study was to measure the spatial variability of vertical fluxes and investigate the relationship between BNL formation and sinking particles. We aimed to determine the particle concentration of POC, Chl *a* and bSi on the Agulhas Bank. We further aimed to measure the proportion of exported organic carbon generated through primary production (export efficiency or ExEff) and the fraction of exported organic carbon flux that reaches the bottom of the water column

(transfer efficiency or TE), to be able to confirm that sinking phytodetritus may contribute to a BNL formation. We hypothesized that there would be a link between the sinking particulate organic matter and the presence of high bottom turbidity (a proxy for BNL).

## 2. Methods

### 2.1. Study area

This study was conducted in the Western Indian Ocean’s eastern and central Agulhas Bank, between Port Alfred and Mossel Bay area (Fig. 1) onboard the RV *Ellen Khuzwayo* during 23–31 March 2019 research cruise (Noyon, 2019). The hydrography of the Agulhas Bank has a marked seasonal variation and differences in the thermal structure between the CAB and EAB (Largier and Swart, 1987; Roberts et al., this issue; Schuman and Beekman, 1984). The EAB is characterized with the intense, shallow thermoclines with gradients of  $10 \text{ }^\circ\text{C}$  over 10 m in summer, resulting from the vertical turbulent mixing of the water column (Boyd et al., 1992; Largier and Swart, 1987). In winter, the upper mixed layer cools down to  $16\text{--}17 \text{ }^\circ\text{C}$  and deepens due to the prevailing westerlies and associated swells: weakening the thermal structure on the EAB (Largier and Swart, 1987). The CAB thermal structure differs from the EAB by being more isothermal on the inner and mid-shelf during winter (Largier and Swart, 1987). Flow patterns on the Agulhas Bank are very complex (Boyd and Shillington, 1994). The CAB is characterized by weak currents, and the presence of the cold-ridge which is associated with high productivity (Boyd et al., 1992; Largier and Swart, 1987), as mentioned previously. The detailed hydrological conditions of the Agulhas Bank are reviewed in (Roberts et al., this issue).

Seawater samples were collected using two Marine Snow Catchers (MSCs); see below for brief description of how the MSC works. Transects were numbered from 1 to 12 (east to west) and stations 1 to 6 (inshore to offshore). We sampled 15 stations at two depths: the export depth which was below the surface mixed layer (SML); to gauge what was exported from the surface ocean, and the bottom depth which was determined by visually viewing the highest bottom turbidity from the CTD’s profiles; to investigate how much of the exported material reached the bottom and to note the presence and/or absence of the benthic nepheloid layer (Fig. 1, Table S1). The SML depth was determined from the CTD’s profiles (see Poulton et al., this issue) and ranged between 7 and 27 m. Stations 1.1, 5.1, 7.1 and 7.2 were only sampled at the bottom MSCs because of their shallow depth. In addition, a Seabird 911+ V2 CTD system coupled with Seabird 32 Rosette with 12 Niskin bottles, equipped

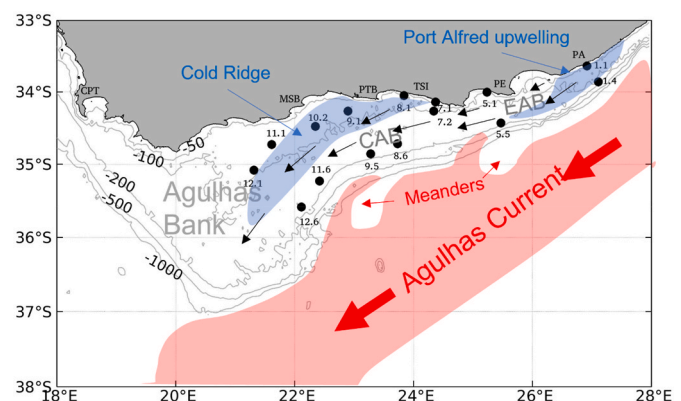


**Fig. 1.** Map of the study site with bathymetry of 100–1000 m showing the southward fast-flowing Agulhas Current (AC) which lies on the shelf edge of the Eastern Agulhas Bank (EAB) and Central Agulhas Bank (CAB) of South Africa. Fifteen stations were sampled using two MSCs and a CTD during the SOLSTICE March 2019 cruise. PA = Port Alfred, PE = Port Elizabeth (now Gqeberha), TSI = Tsitsikamma, PTB = Plettenberg Bay, MSB = Mossel Bay and CPT = Cape Town.

with an Optical Backscatter Sensor (OBS-3+) was used to measure turbidity. We used a threshold of  $>1.7$  nephelometric turbidity units (NTUs) based on [Biscaye and Eitrem \(1977\)](#) as the standard for BNL presence.

The MSC is a large volume (95 L) water sampler with detachable top and bottom/base sections. The bottom of the base chamber was used to attach the tray which has a 1 L volume capacity. The measured tray volume may vary depending on the amount of water captured in a tray. During deployment, the sections of the MSC are joined together using side metal clips, and the terminal apertures of the water sampler are left open to allow water movement through the cylinder with minimal turbulence. Upon reaching the desired depth, the MSC is closed by releasing a messenger. The MSC is then retrieved to the surface and secured on the ship's deck for the particles to settle onto the base and tray. Right after MSC retrieval, water samples are collected from the top section of the MSC as "time-zero". After 2 h of MSC settling time (time-final), water from the top section is drained into a 5 L container through the bottom tap to minimize resuspension of particles for the estimation of the suspended particle concentration. The top section is then detached from the base of the MSC. The water in the base of the MSC is examined for any visible aggregates or large marine snow particles. Water from the base is siphoned into a container for the estimation of slow-sinking particle concentration. The tray is removed from the base and the water is transferred into a container for the estimation of the fast-sinking particle concentration. Detailed information about the functioning of the MSC is in ([Giering et al., 2016](#); [Riley et al., 2012](#)).

## 2.2. Sample analysis

### 2.2.1. Particulate organic carbon (POC)

Typically, 1100 mL of seawater was filtered onto pre-combusted (450 °C for 24h) MF 300 glass fibre filters (nominal pore size 0.7  $\mu\text{m}$ , 25 mm diameter) in duplicates. For fast-sinking samples, 150–300 mL was filtered. After rinsing the filter with pH adjusted distilled water (pH 8.5, 180  $\mu\text{L}$  25% ammonium in 1 L distilled), filters were dried in the oven overnight at 50 °C and stored until analysis on shore. On shore, filters were fumed with 35% hydrochloric acid for 24 h to remove any inorganic carbon, dried (50 °C,  $>24$  h) and pelleted in tin disks. The samples were analysed for POC using a Thermo Fisher Scientific FLASH 2000 Organic Elemental Analyser coupled to a Delta V Advantage Isotope Ratio Mass Spectrometer (IRMS). All samples were blank-corrected.

### 2.2.2. Chlorophyll *a* (Chl *a*)

Typically, 200 mL of seawater was filtered onto glass-fibre filters (Fisherbrand MF300 nominal pore size 0.7  $\mu\text{m}$ , 25 mm diameter). The volume of seawater filtered from the tray fraction ranged from 90 to 200 mL per sample. Filters were placed in 6 mL of 90% acetone (Sigma-Aldrich, UK) at 4 °C for 18–24 h to facilitate pigment extraction. Chl *a* was measured on a Turner Designs Trilogy fluorometer using a non-acidification module (see [Welschmeyer, 1994](#)) calibrated with solid and pure Chl *a* standards (Sigma-Aldrich, UK).

### 2.2.3. Biogenic silica (bSi)

Typically, 500 mL of seawater was filtered onto Whatman polycarbonate filters (0.8  $\mu\text{m}$  pore size, 25 mm diameter). Filters were rinsed with pH-adjusted distilled water to remove salts. Samples were placed into 15 mL tubes, dried at 50 °C in an oven and stored for later analysis. In the laboratory, filters were digested with 5 mL of 0.2 M NaOH at 85 °C for 2 h ([Ragueneau and Tréguer, 1994](#)). After cooling, filters were neutralized with 1 mL of 1.0 M HCl (pH 7–8.5). Samples were centrifuged at 2500 rpm for 10 min to allow the separation of supernatant from the suspended material. Silicate was then analysed in an auto analyser (SEAL analytical AACE 7.03). The auto analyser was calibrated with a silica stock solution of 10 000  $\mu\text{mol/L}$ . A working solution with a final concentration of 100  $\mu\text{mol/L}$  was prepared from the original silica stock solution to prepare calibrants. A Certified Reference Material

(KANSO Co., LTD, Japan) was used to check precision and accuracy of the instrument. All samples were blank- and drift-corrected. Baseline, artificial seawater, and wash solution were prepared with MilliQ water, filtered through Whatman polycarbonate filters (0.2  $\mu\text{m}$  pore size, 47 mm diameter). Calibrants were prepared with artificial seawater (35g of sodium chloride plus 0.2g of hydrogen carbonate were dissolved in 1 L Milli Q water). All reagents were prepared in plasticware to prevent silica contamination. Measured bSi values were converted to silica by assuming a molar mass of 67 g/mol (see [Mortlock and Froelich, 1989](#)).

## 2.3. Particle calculations

### 2.3.1. Particle concentration and fluxes

Concentrations of suspended, slow-sinking, and fast-sinking particles were calculated as below based on the previous studies ([Baker et al., 2017](#); [Riley et al., 2012](#)):

$$P_{suspended} = P_{top} \quad (1)$$

$$P_{slow} = (P_{bottom} - P_{top}) \times V_{base} / V_{MSC} \quad (2)$$

$$P_{fast} = (P_{tray} - P_{bottom}) \times (V_{tray} / 1000) / (A_{tray} \times h_{MSC} \times 1000) \quad (3)$$

where  $V_{base}$  is the volume of the base section of the MSC (8 L),  $V_{MSC}$  is the volume of the MSC (95 L including the base) and  $V_{tray}$  is the volume of the water available in a tray (mL),  $A_{tray}$  is the area of the tray, (0.026  $\text{m}^2$ ),  $h_{MSC}$  the height of the MSC (1.58 m) and 1000 is a conversion number for the units.

Fluxes for slow-sinking ( $F_{SS}$ ) and fast-sinking ( $F_{FS}$ ) particles were calculated as follows:

$$F_{SS} = P_{slow} \times V_{MSC} / (A_{MSC} \times t) / 1000 \quad (4)$$

$$F_{FS} = P_{fast} \times V_{fast} \quad (5)$$

where  $A_{MSC}$  is the area of the MSC base (0.06  $\text{m}^2$ ),  $t$  is the settling time of the MSC (2 h) and  $V_{fast}$  is the particle sinking speed (60  $\text{m d}^{-1}$ ). The particle sinking speed in previous studies ranged from 50 to 2000  $\text{m d}^{-1}$ , with areas influenced by spring blooms having the higher sinking speed ([Giering et al., 2016](#); [Riley et al., 2012](#)). The authors determined the sinking particle speed by manually picking visible aggregates of greater than 0.5 mm diameter and dropping them in a cylinder, while timing the settling time of the aggregate. Due to the lack of visible aggregates, our aggregate sinking speed was decided based on the previous literature reviews ([Belcher et al., 2016](#); [Giering et al., 2016](#); [Omand et al., 2020](#)) and on the plankton composition during the cruise. Phytoplankton composition during the cruise was dominated by small phytoplankton, with less diatoms and few large Chl *a* aggregates ([Poulton et al., this issue](#); [Giering et al., this issue](#)), likely to result in low sinking particles.

### 2.3.2. Export efficiency (ExEff) and transfer efficiency (TE)

Export efficiency (ExEff) is the efficiency at which POC, generated through primary production, gets transported from the surface to the ocean interior and is a good metric for the strength of the biological carbon pump ([Ceballos-Romero et al., 2016](#)). ExEff was calculated following [Ceballos-Romero et al. \(2016\)](#), using an average of 9 m below the surface mixed layer as the reference depth for the export flux as follows:

$$ExEff = (POC \text{ export flux}) / NPP, \quad (6)$$

where POC export flux was the flux measured on average of 9 m below the surface mixed layer and NPP was estimated based on surface-calibrated chlorophyll concentrations (see [Poulton et al., this issue](#)). The NPP depth used here was similar to that of POC export flux. Stations 1.1, 5.1 and 7.1 were omitted from the calculations because they only had deep MSCs.

Transfer efficiency (TE), which is the fraction of exported organic carbon that reaches the bottom depth was adopted from the Martin curve power law (Martin et al., 1987). We used the power law to estimate the flux at 2 different fixed depths, and calculated TE following Buesseler et al. (2020). We used 100 m depth as the bottom flux reference depth and 30 m as the export flux reference depth. The 30 m reference was chosen because it was below the SML (average SML = 18 m), so it was appropriate for estimated flux. The bottom reference was appropriate as most of the bottom MSCs depths were in-between 30 and 100 m (Table S1) and below the euphotic zone maximum of 62 m (Poulton et al., this issue). Transfer efficiency at each station (excluding stations with 1 MSC) was calculated using the following equation was:

$$TE = (Flux_{100}) / (Flux_{30}) \quad (7)$$

Where flux was the flux of POC, Chl a or bSi, respectively.

### 2.4. Data analyses

All statistical analyses were performed in R statistical software version 3.6.1 (R Core Team, 2019). Welch's t-test was used to compare the differences in the distribution of fluxes between inshore and offshore. We used Kruskal-Wallis and comparison test to determine the differences in particle concentration by fraction from the export and bottom MSCs. Furthermore, Wilcoxon test was used to assess the distribution of particle concentration between export and bottom samples. We log-transformed bottom turbidity and fluxes data and used linear regression to explore the relationship between bottom turbidity and export fluxes.

## 3. Results

### 3.1. Particle fluxes

Overall, there was a decrease in fluxes with depth (Fig. 2). The flux range for POC, Chl a and bSi was as follows: 208.06–1947.71 mg m<sup>-2</sup> d<sup>-1</sup>, 0.15–10.65 mg m<sup>-2</sup> d<sup>-1</sup> and 0–60 mg m<sup>-2</sup> d<sup>-1</sup>, respectively (Fig. 2). Port Alfred recorded the highest fluxes compared to the rest of the Agulhas Bank (Figs. 2 and 3). POC export fluxes were significantly

higher inshore than offshore (Welch's t-test, p < 0.01; mean ± SD: 944.6 ± 302.0 & 461.1 ± 162.1 mg m<sup>-2</sup> d<sup>-1</sup>, respectively). Even though Chl a and bSi export fluxes were not significantly different, they were still higher inshore than offshore (mean ± SD<sub>Chl a</sub>: 2.8 ± 1.8 & 1.5 ± 0.7 mg m<sup>-2</sup> d<sup>-1</sup>, respectively, and mean ± SD<sub>bSi</sub>: 9.5 ± 9.4 & 9.2 ± 11.2 mg m<sup>-2</sup> d<sup>-1</sup>, respectively; see Table S2). All the bottom fluxes were significantly higher inshore than offshore (Welch's t-test, p < 0.05 & p < 0.01; Table S2, Fig. 4b, d and f). The sample size of inshore fluxes was bigger than that of offshore fluxes for all the parameters (Table S2).

### 3.2. POC, Chl a and bSi concentration of suspended, slow, and fast sinking particles

The concentration of POC averaged across the export MSCs (±S.D.) for suspended, slow- and fast-sinking particles was 107.20 (±48.58), 10.13 (±5.64) and 7.71 (±3.81) µg L<sup>-1</sup>, respectively (Table S3). The particle contribution to total POC concentration was 84%, 9% and 7% for suspended, slow- and fast-sinking particles, respectively (Fig. 5a). The bottom MSCs had an average POC concentration of 61.96 (±39.14), 5.13 (±2.78) and 5.09 (±2.54) µg L<sup>-1</sup> for suspended, slow- and fast-sinking particles, respectively (Table S3). The particle contribution to POC concentration by the bottom MSCs was 84%, 8% and 8% for suspended, slow- and fast-sinking particles, respectively.

The average Chl a concentration in the export MSCs was 1.22 (±0.66), 0.03 (±0.03) and 0.02 (±0.02) mg m<sup>-3</sup> for suspended, slow- and fast-sinking particles, respectively. The particle contribution to total Chl a concentration in the export MSCs was 94%, 4% and 2% for suspended, slow- and fast-sinking particles, respectively. Bottom MSCs had an average Chl a concentration of 0.43 (±0.83), 0.01 (±0.02) and 0.01 (±0.01) mg m<sup>-3</sup> for suspended, slow- and fast-sinking particles, respectively. The particle contribution to total Chl a concentration was 89%, 3% and 8% for suspended, slow- and fast-sinking particles, respectively (Table S3).

For bSi, we measured an average concentration of 2.059 (±1.60), 0.038 (±0.10) and 0.143 (±0.17) µg L<sup>-1</sup> for suspended, slow- and fast-sinking particles in the export MSCs. The contribution of particles to total bSi concentration in the export MSCs was 90%, 4% and 6% for suspended, slow- and fast sinking particles, respectively (Table S3). The

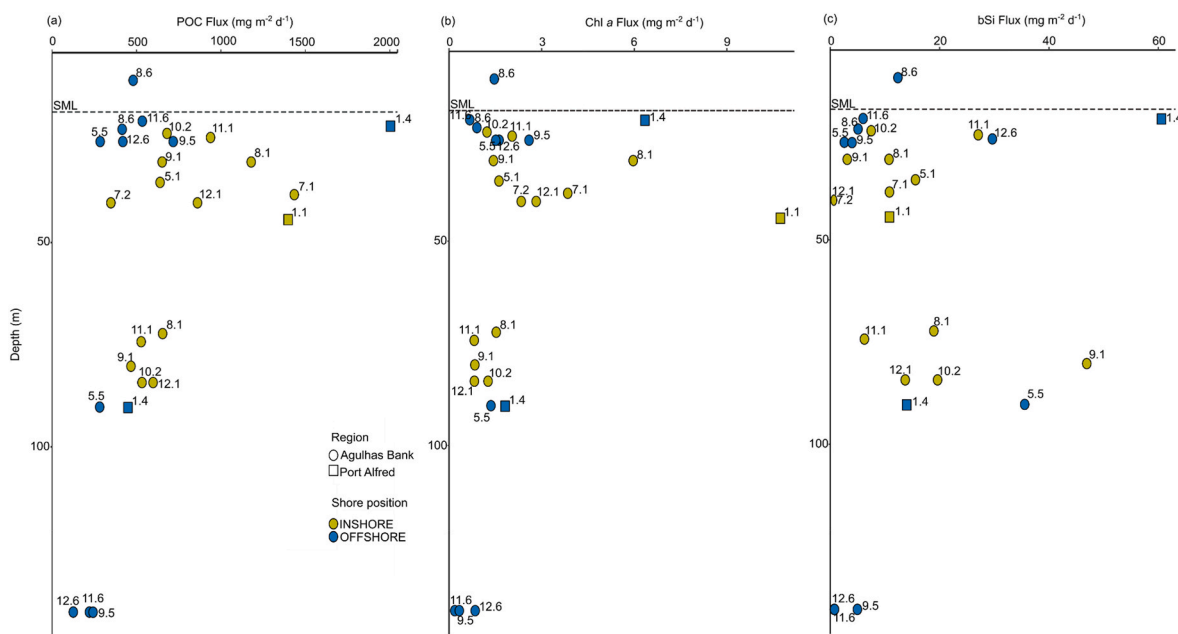


Fig. 2. Vertical fluxes of Particulate Organic Carbon (mg m<sup>-2</sup> d<sup>-1</sup>) (a), Chlorophyll a (mg m<sup>-2</sup> d<sup>-1</sup>) (b) and biogenic Silica (mg m<sup>-2</sup> d<sup>-1</sup>) (c) on the Agulhas Bank (circles) and Port Alfred (squares) during the SOLSTICE 2019 cruise. Inshore stations are indicated by green symbols and offshore stations are blue symbols. The dotted line represents the average surface mixed layer (SML) depth.

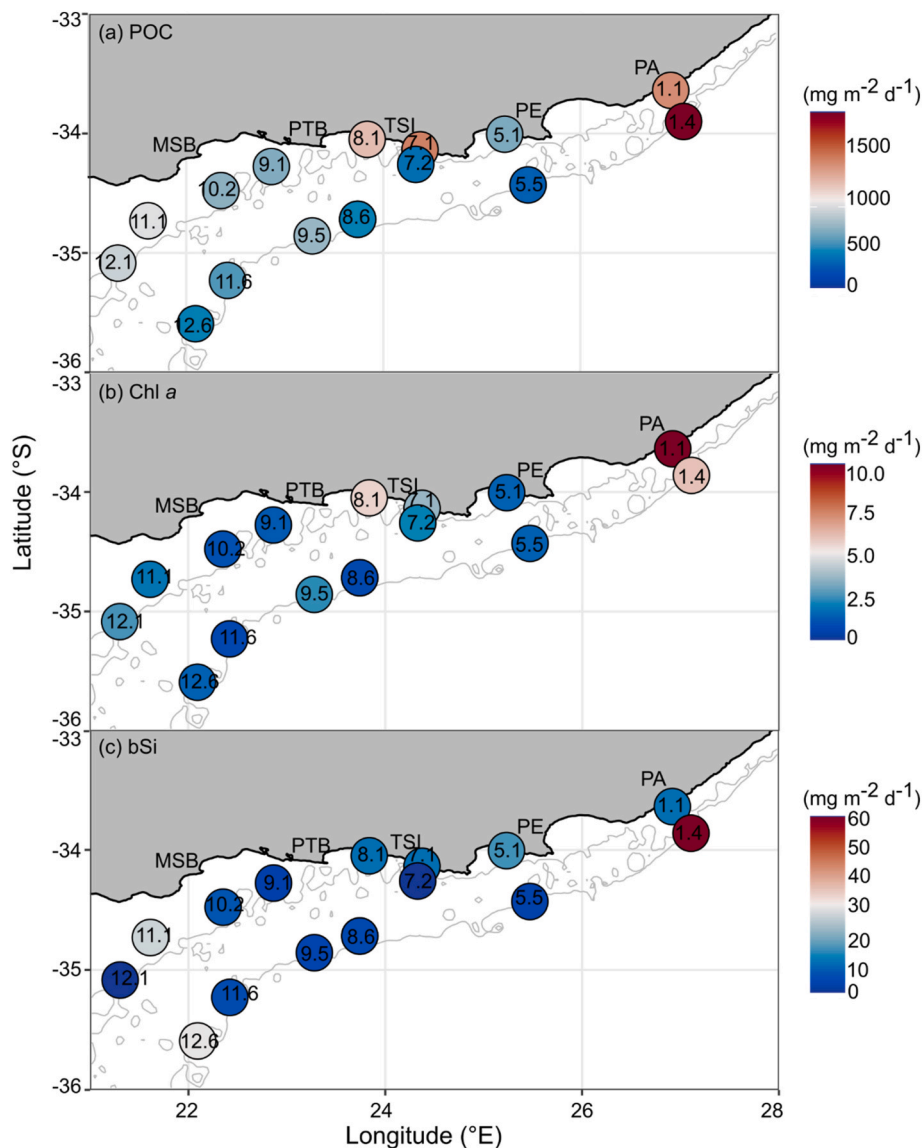


Fig. 3. Spatial distribution of export fluxes of POC (a), Chl *a* (b) and bSi (c) in  $\text{mg m}^{-2} \text{d}^{-1}$ . The map shows the bathymetry at 100 m and 200 m isobaths. The circles and colour bars indicate surface fluxes. PA = Port Alfred, PE = Port Elizabeth (Gqeberha), TSI = Tsitsikamma, PTB = Plettenberg Bay and MSB = Mossel Bay.

bottom MSCs showed an average bSi concentration of  $1.84 (\pm 1.50)$ ,  $0.05 (\pm 0.13)$  and  $0.44 (\pm 0.63) \mu\text{g L}^{-1}$  for suspended, slow- and fast-sinking particles, respectively. The proportion of particle contribution to total bSi in the bottom MSCs was 80%, 4% and 16%, for suspended, slow- and fast sinking particles, respectively. Overall, the particle concentration decreased with depth except for bSi slow and fast sinking particle concentration which increased in the bottom MSCs (Table S3).

### 3.2.1. Particle stoichiometry

Overall, the range of concentration ratios was higher in the export (Chl *a*:POC: 0–0.02 and Chl *a*:bSi: 0–3.34) compared to bottom MSCs (Chl *a*:POC: 0–0.01 and Chl *a*:bSi: 0–2.73), except for bSi:POC ratio which was higher in the bottom than export (maximum: 0.03 and 0.02, respectively, Fig. 6). The mean Chl *a*:POC and Chl *a*:bSi concentration ratio was higher in the suspended fraction of the export MSCs than in other fractions (mean  $\pm$  SD:  $0.011 \pm 0.004$  and  $0.814 \pm 0.730$ , respectively). For bSi:POC, the mean concentration ratio was higher in the fast-sinking fraction of the bottom MSCs (mean  $\pm$  SD:  $0.008 \pm 0.010$ ). The lowest mean concentration ratio was measured in the slow-sinking fraction of the bottom MSCs for Chl *a*:POC, and fast-sinking fraction of the bottom MSC for Chl *a*:bSi (mean  $\pm$  SD:  $0.002 \pm 0.003$

and  $0.061 \pm 0.044$ , respectively). The lowest mean bSi:POC concentration ratio was found in the slow-sinking fraction of export MSC (mean  $\pm$  SD:  $0.001 \pm 0.001$ ).

The export MSCs Chl *a*:POC and bSi:POC particle concentration significantly differed between fractions (i.e., suspended, slow- and fast-sinking) as determined by the Kruskal-Wallis test ( $p < 0.0001$  &  $p < 0.05$ , respectively). Chl *a*:bSi particle concentration of the export MSCs was not significantly different between fractions. The particle concentration ratios of the bottom MSCs did not show any significant differences between fractions. The particle concentration of Chl *a*:POC in the export MSCs was always significantly higher in the suspended fraction than in the fast- and slow-sinking fractions, as determined by the pairwise-comparison test ( $p < 0.001$  and  $p < 0.01$ , respectively). For bSi:POC particle concentration of the export MSCs, the significant differences were observed between slow- and fast-sinking fractions, and slow-sinking and suspended fractions ( $p < 0.05$ ).

### 3.3. Export efficiency (ExEff) and transfer efficiency (TE)

POC ExEff ranged from 0.58 to 9.26 (Fig. 7a). Station 11.1 had the highest ExEff, followed by the station offshore Port Alfred with the

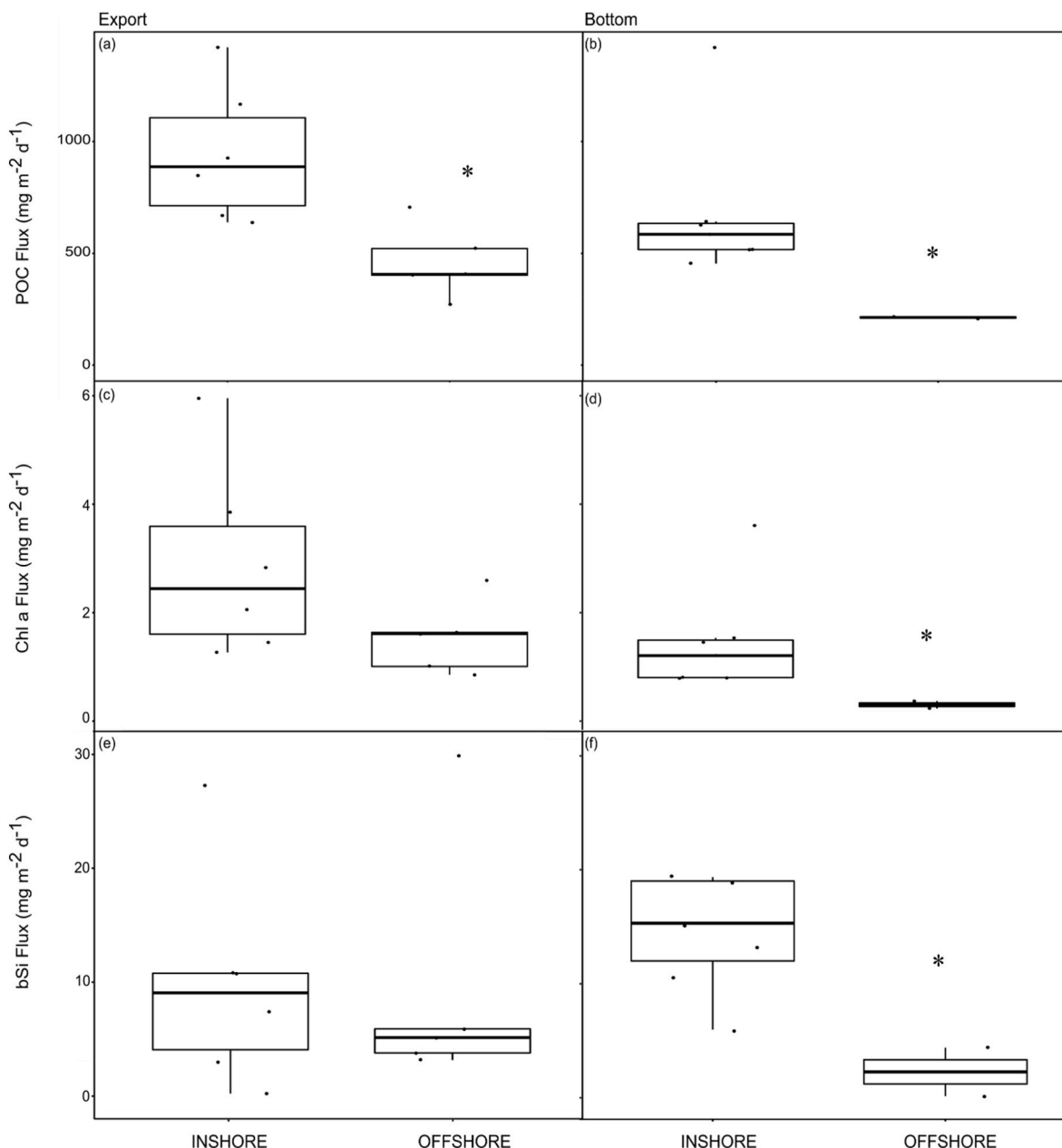


Fig. 4. Inshore-offshore comparison of POC, Chl *a* and bSi fluxes of the export (a, c, e) and the bottom depths (b, d, f). The asterisks indicate the level of significant difference at 0.05 between inshore and offshore fluxes. Port Alfred transect was excluded from the analysis because of very high fluxes to avoid bias.

efficiency of 6.5. The lowest ExEffs were observed at stations 5.5, 8.6 and 12.6 (0.7, 0.7 and 0.6, respectively). There were no significant differences in the cross-shelf distribution of ExEff; however, inshore had higher mean values than offshore (Median  $\pm$  SD<sub>inshore</sub>: 2.13  $\pm$  3.35 and Median  $\pm$  SD<sub>offshore</sub>: 0.68  $\pm$  0.50, Fig. 7b). The range of POC TE was 30–99%, Chl *a* TE: 15–100% and bSi TE: 20–330% (Fig. 8). Unlike the ExEff, TE of the three parameters was low off Port Alfred stations and did not show a spatial pattern. There was no clear inshore-offshore trend in the TE of POC, Chl *a* and bSi (Welch’s *t*-test: *p* = 0.91, *p* = 0.96 & *p* = 0.48, respectively).

#### 4. Discussion

##### 4.1. Fluxes

The fluxes discussed in this section are those of POC as it plays an important role in understanding the biological carbon pump dynamics

in this region. The Agulhas Bank recorded high fluxes ranging from 208 to 1948 mg m<sup>-2</sup> d<sup>-1</sup> which are comparable to the global POC fluxes measured at depths of <220 m between 1985 and 2013 (0–1500 mg m<sup>-2</sup> d<sup>-1</sup>). These were higher in the shelf regions and high latitudes (Le Moigne et al., 2013). POC fluxes are influenced by primary production resulting from the abundance of inorganic nutrients induced by upwelling, runoff or remineralization, which leads to the increased vertical transport of organic matter (Banse and English, 2000; Reigstad et al., 2008). Although the Agulhas Bank is known as a productive region (1998–2018 timeseries monthly average daily NPP of 0.12–11.08 g C m<sup>-2</sup> d<sup>-1</sup>; Mazwane et al., this issue); there was moderate primary production during the cruise (daily NPP of 0.1–1.1 g C m<sup>-2</sup> d<sup>-1</sup>; Poulton et al., this issue), suggesting that our high POC fluxes might have been influenced by other factors besides primary production. Factors such as the presence of large phytoplankton (e.g. diatoms) which contribute to the vertical carbon transfer by ballasting with POC or by being incorporated in zooplankton fecal pellets, can enhance POC fluxes (Francois

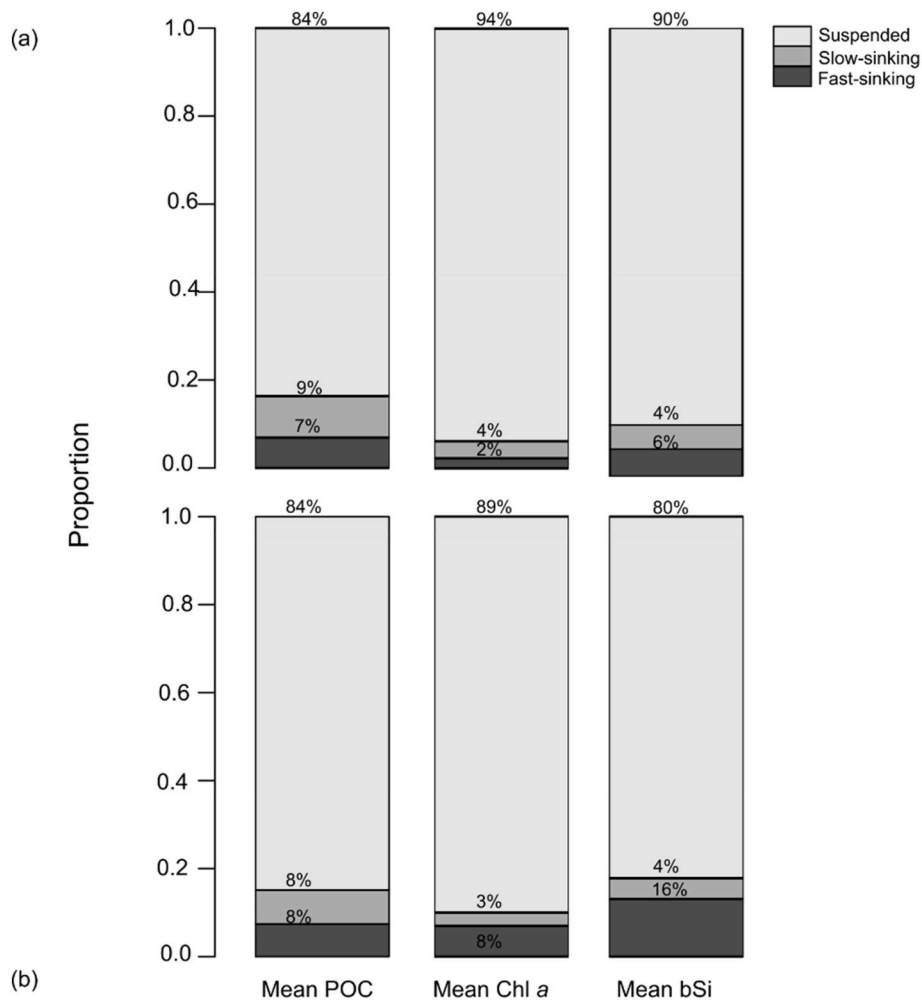


Fig. 5. Proportion of average concentration of (a) Particulate Organic Carbon (POC in  $\mu\text{g L}^{-1}$ ) chlorophyll (Chl *a* in  $\mu\text{g L}^{-1}$ ) and biogenic silicate (bSi in  $\mu\text{g L}^{-1}$ ) in the export and (b) bottom stations indicated by percentages. Light grey indicates suspended particles, grey is slow-sinking particles and dark grey indicates fast-sinking particles. Station 1.4 was excluded from the analysis because of very high concentrations to avoid bias.

et al., 2002; Klaas and Archer, 2002).

While the Agulhas Bank fluxes, overall, are comparable to the global shelf seas, our results showed that the Agulhas Bank experienced high spatial variability, with the Port Alfred region experiencing maximum surface fluxes when compared to the rest of the shelf ( $1948 \text{ mg POC m}^{-2} \text{ d}^{-1}$ , Figs. 2 and 3), with a distinct cross-shelf difference. The high variability in fluxes that we observed can likely be explained by the oceanographic complexity of the Agulhas Bank region (Lutjeharms et al., 2000; Probyn et al., 1994; Roberts and van den Berg, 2005; Swart and Largier, 1987), with the Port Alfred region being influenced by the enhanced wind-driven coastal upwelling (Lutjeharms et al., 2000). During upwelling events, nutrient-rich water at depth is introduced into the surface, allowing phytoplankton abundance to increase (Bakun, 1973; Lutjeharms et al., 2000; Swart and Largier, 1987; Yokomizo et al., 2010). The abundance of phytoplankton can lead to high carbon fluxes due to the sinking of relatively large aggregates and fecal pellets in areas where there is low organic matter degradation by zooplankton and microbes (Aldredge and Silver, 1988; Bach et al., 2019; Fowler and Knauer, 1986; Muller-Karger et al., 2004).

Although there were low concentrations of surface-mixed layer nitrate and nitrite ( $<1 \mu\text{M}$ ) and intermediate surface NPP ( $<0.6 \text{ g C m}^{-2} \text{ d}^{-1}$ ) off Port Alfred during the cruise (Poulton et al., this issue), to link fluxes to upwelling events; the presence of a high abundance of Chl *a* spikes in the upper water column suggested a post-upwelling scenario (Giering et al., this issue). The post-upwelling is characterized by large

aggregates of phytodetritus which sink faster to the bottom, high abundance of small-sized phytoplankton and low nutrient concentrations (Fowler and Knauer, 1986; Krause et al., 2019; Kudo et al., 2000; Millan-Nuñez et al., 1982; Shin et al., 2017). The surface phytoplankton community in the Agulhas Bank was dominated by pico-sized ( $0\text{--}2 \mu\text{m}$ ) phytoplankton and micro phytoplankton ( $>20 \mu\text{m}$ ) (Poulton et al., this issue), typical of an end of the upwelling phase. Also, satellite-derived surface Chl *a* concentration and sea surface temperature (SST) data showed an increase in surface Chl *a* concentration and low SST off Port Alfred, extending to the outer shelf a week before the cruise (see Figs. S5–S7); suggesting the possibility of an upwelling event which would result in enhanced primary production. Therefore, we suggest that the high fluxes observed off Port Alfred were derived from the sinking of large phytodetritus aggregates derived from a bloom that occurred before the cruise.

The other factor that might influence high POC fluxes observed off Port Alfred is the ‘ballasting effect’ of bSi with POC (Armstrong et al., 2002). The ballasting of biogenic silica, derived from diatoms and other silica containing phytoplankton, aids in the vertical transport of POC to deeper ocean layers, by producing dense fast-sinking particles, which are resistant to microbial degradation (Armstrong et al., 2002; Franco et al., 2002; Klaas and Archer, 2002). We observed higher surface bSi fluxes off Port Alfred and an intermediate surface diatom cell abundance of about  $3000\text{--}4000 \text{ cells L}^{-1}$  (Poulton et al., this issue), which was higher than the rest of our stations (except for 8.6, 9.5 and 12.6),

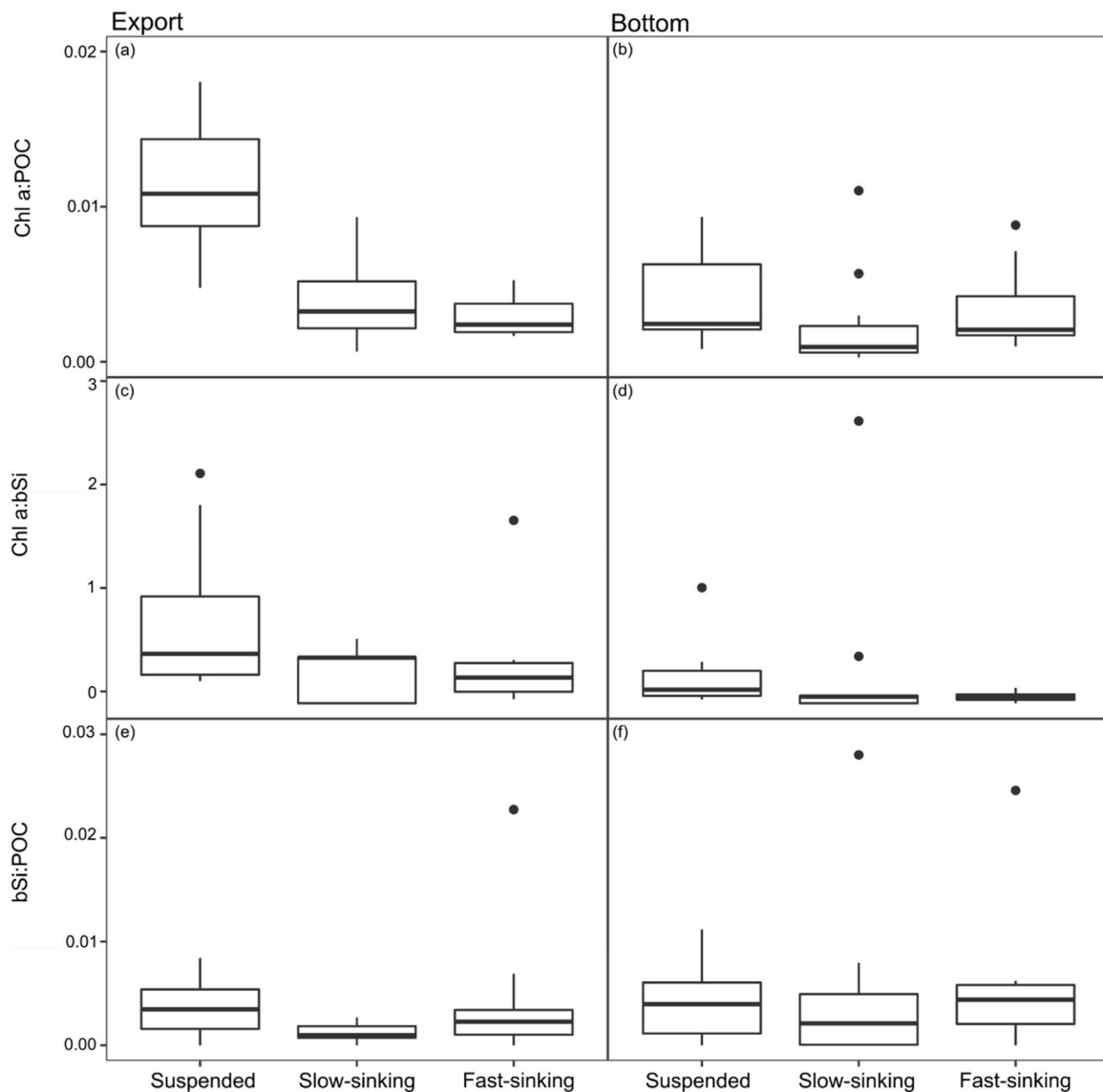


**Fig. 6.** Concentration ratio of Chl *a*:POC (mg:mg), Chl *a*:bSi (mg:mg) and bSi:POC (mol:mol) for suspended, slow-sinking and fast-sinking particles in export (a, c & e) and bottom (b, d & f) MSCs. Station 1.4 was excluded from the analysis because of very high concentrations to avoid bias.

suggesting the possibility of a ballasting effect. Fresh diatoms are known to float, while decaying diatoms sink faster to the bottom in the form of large aggregates (Krause et al., 2019). Unfortunately, the size fractionated Chl *a* fraction was not measured at station 1.4 (Poulton et al., this issue). Even though other biological factors that might influence POC fluxes were not measured, we suggest that high POC fluxes observed off Port Alfred were influenced by the vertical transport of post-bloom derived phytodetritus, likely enhanced by ballasting with bSi.

The second major trend observed on the AB was the significantly higher POC fluxes inshore when compared to offshore in both export and bottom MSCs (Fig. 4a and b). This section excludes the Port Alfred region due to its distinctive biophysical dynamics that differ from the rest of the Agulhas Bank. Similar differences in cross-shelf POC flux distribution have been observed elsewhere: the Arabian Sea shelf (Lee et al., 1998), the Guatemala coast (Cavan et al., 2017), and the East China Sea shelf (Iseki et al., 2003). Cross-shelf flux distribution is influenced by primary productivity, riverine input and sediment resuspension which decrease towards offshore regions (Fan et al., 2018; Iseki et al., 2003; Lee et al., 1998). We expected the inshore of the Agulhas Bank to have higher fluxes because of its productive upwelling events.

During our cruise there were no cross-shelf gradients in surface NPP

and surface Chl *a* concentration (Poulton et al., this issue), to explain this trend. Even though we did not observe a cross-shelf NPP gradient, a 20-year satellite-derived annual NPP confirmed a high inshore-low offshore NPP trend (Mazwane et al., this issue). Also, Chl *a* flux was higher inshore than offshore from the AB in both MSC depths (Fig. 4c and d). Therefore, it is possible that this high inshore Chl *a* flux contributed to cross-shelf differences of POC fluxes observed on the AB.

An alternative explanation for high inshore POC fluxes in the bottom MSCs would be the resuspension of sediments, as our inshore bottom MSCs depth range was 0–8 m above the bottom (except station 7.2) while offshore bottom MSCs ranged from 5 to 106 m above the bottom, making inshore MSCs susceptible to resuspended sediments. The Agulhas Bank is influenced by bottom currents which are capable of resuspending sedimentary organic matter (Roberts and Sauer, 1994; Roberts and van den Berg, 2005; Zoutendyk and Duvenage, 1989), therefore intensifying POC fluxes by ballasting (Fan et al., 2018). A simultaneous study which was investigating particle assemblages based on their optical properties' composition on the AB, confirmed that there was elevated red backscatter intensity near-bottom in the inshore stations during the cruise, suggesting suspended sediments (Figs. 4 and 8a; Giering et al., this issue). To further explain ballasting of resuspended

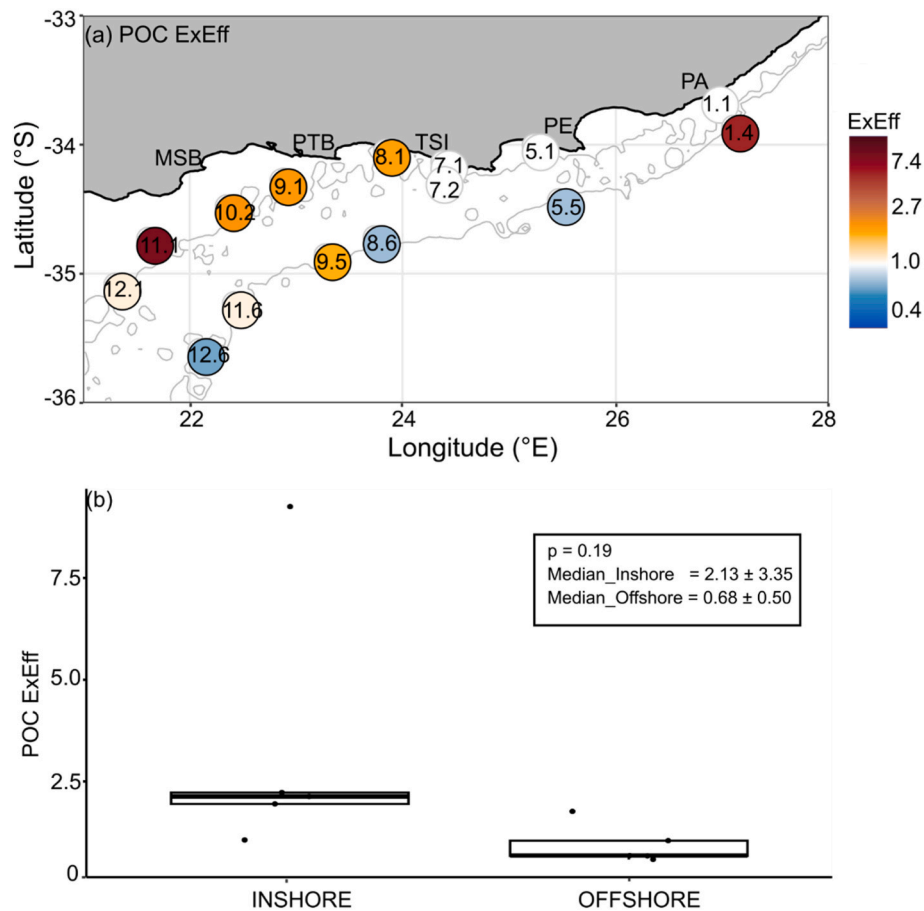


Fig. 7. Spatial distribution of POC Export efficiency (ExEff) proportion (a) and inshore-offshore comparison of POC ExEff on the Agulhas Bank (excluding Port Alfred) (b). Colour bar indicates proportion values of ExEff at each station.

sediments with POC, we observed significantly higher bSi fluxes inshore than offshore in the bottom MSCs (Fig. 4f), suggesting the possibility of ballasting of resuspended sediments rich in bSi with POC. This indicates that resuspension of sediments might have been a factor influencing high bSi fluxes as these fluxes were higher than those of the inshore export MSCs (Fig. 4e). Therefore, we suggest that the cross-shelf gradient POC flux of the export MSCs was likely due to primary production which might have occurred prior to the cruise as shown by the satellite images, while the bottom MSCs cross-shelf gradient might have been influenced by the resuspended bottom sediments.

#### 4.2. Contribution of sinking particles to concentration and fluxes of POC, Chl *a* and bSi on the Agulhas Bank

In terms of the export particle composition (excluding Port Alfred), slow-sinking particles contributed slightly more to POC and Chl *a* concentration (9% and 4%, respectively, Fig. 5a) than fast-sinking particles (7% and 2%, respectively). This was expected as the Agulhas Bank phytoplankton composition was dominated by nanoplankton and picoplankton (average: 45% and 29%, respectively; Poulton et al., this issue), with few large aggregates (Giering et al., this issue). Generally, an abundance of fast-sinking particles would be found in regions dominated by micro phytoplankton such as diatoms which sink faster to the bottom. It is evident from our bSi:POC concentration ratio that POC concentrations on the Agulhas Bank were not largely influenced by the siliceous phytoplankton at the time of sampling (for e.g., diatoms), as our range of bSi:POC was lower (0–0.03 mol:mol) than an average diatom Si:C of 0.13 mol:mol (Fig. 6e and f, Brzezinski, 1985). High bSi:POC ratios are usually associated with areas occupied by siliceous

phytoplankton and dominated by diatoms (Leynaert et al., 1991). It is not surprising that we observed low bSi:POC ratio as we sampled post-bloom when phytoplankton community was dominated by small phytoplankton groups. Since most of the phytoplankton was small and suspended, the sinking particle fraction might have formed through biological particle aggregation or the particle coagulation of sinking or suspended small particles to produce dense aggregates (Taucher et al., 2018). The observed POC particle concentration trend is comparable to a few studies which suggested that slow-sinking particles contribute more to POC concentration than fast-sinking particles (Baker et al., 2017; Giering et al., 2016; Riley et al., 2012).

For the export bSi concentration, fast-sinking particles contributed slightly more to the sinking particle fraction than slow-sinking particles (6% and 4%, respectively, Fig. 5a). This pattern differed from that of POC and Chl *a* sinking particle contribution to concentration. This might be due to a higher microbial degradation pressure on POC compared to bSi (DeMaster, 1981; Ragueneau et al., 2006; Subhas et al., 2023). For example, in the euphotic zone, about 35% of bSi can survive dissolution, while less than 4% of organic matter escapes microbial remineralization (DeMaster, 1981). This scenario is likely to occur when diatoms are ballasted with frustules which makes them denser and sink faster (Buesseler et al., 2001). However, our study suggests that there was low contribution by diatoms to phytoplankton community. Also, we did not measure microbial activity to confidently explain the observed bSi sinking particle trend. The high contribution of fast-sinking particles to bSi concentration is not comparable to previous similar studies as they only measured slow-sinking particle fraction for bSi, therefore, further studies are needed to clarify this. (Giering et al., 2016; Riley et al., 2012).

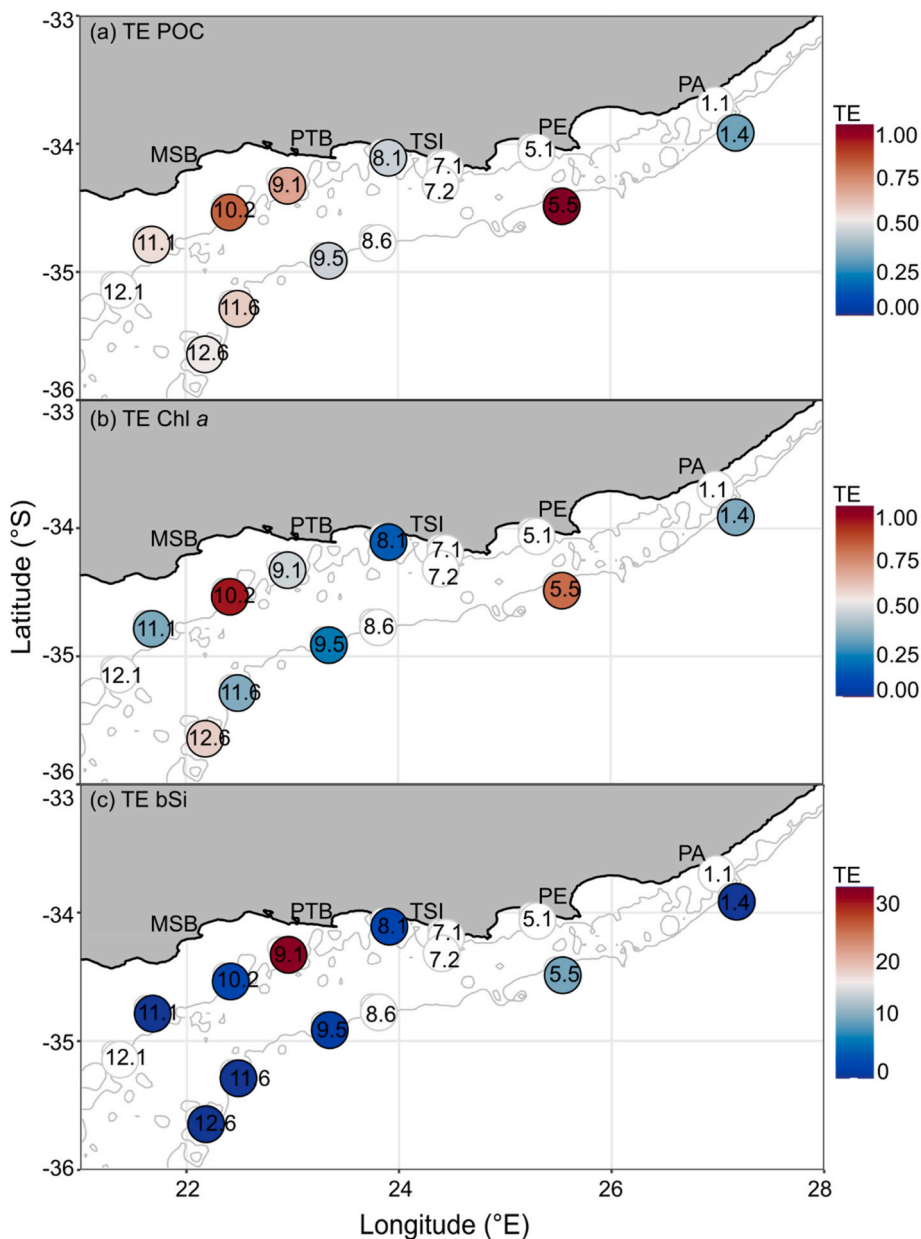


**Fig. 8.** Spatial distribution of POC (a), Chl *a* (b) and bSi (c) transfer efficiency (TE) on the Agulhas Bank and Port Alfred. White circles represent stations where TE was not measured.

While most of the sinking particle contribution to POC concentration in the export MSCs was due to slow-sinking particles; fluxes showed a different pattern, with fast-sinking particles contributing more to POC flux (fast-sinking POC mean ± SD: 462.63 ± 228.29 and slow-sinking POC mean ± SD: 192.55 ± 107.22, Table S4). These findings were not comparable to the previous studies which found a large contribution to POC flux by slow-sinking particles (Giering et al., 2016; Riley et al., 2012). This can be explained by the methodological differences in how we measured the particle sinking speed. We suspect that a large contribution of fast-sinking particles to export fluxes was caused by an aggregation of particles and/or packaging by zooplankton producing fast-sinking fecal pellets that sank on their own or within aggregates (Turner, 2002). Although we can't confirm the production of fecal pellets during the cruise, the AB had an average zooplankton community abundance of 2045 ind.m<sup>-3</sup>, with some stations dominated by large doliolids and calanoids which can produce carbon-rich fecal pellets (Noyon et al., this issue).

Furthermore, we studied the distribution of the sinking particles in the bottom MSCs to determine how it differed from the export MSCs and how much of the export flux reached the bottom. The export and bottom MSC sinking particle contribution to POC concentration was similar, while the concentration of Chl *a* and bSi showed an increase in fast-sinking particles with depth (8% and 16%, respectively, Fig. 5). It is unclear what might have caused an increase of 6% in fast-sinking Chl *a* concentration at the bottom. However, it is possible that the bottom waters from station 8.6 (bottom MSC) which was sampled at a depth of 22 m, might have influenced the increase in Chl *a* observed here. This bottom MSC had a higher Chl *a* concentration due to fast-sinking particles than the export MSC (Table S3). We cannot discuss further the observed sinking particle trend of bSi as mentioned previously.

We observed a decrease in the average particle flux with depth for POC and Chl *a*, but an increase with depth for bSi (Table S4), suggesting decoupling between bSi and other parameters. It is not clear what caused the decoupling between bSi and POC; however, the pattern of

particle flux decreasing with depth is comparable to previous flux studies (Baker et al., 2017; Martin et al., 1987; Riley et al., 2012). The decrease of flux with depth can be explained by numerous factors such as remineralization of POC, fragmentation and grazing on sinking matter (Belcher et al., 2016; Cavan et al., 2017; Turner, 2015). An extensive dataset measuring all the factors influencing POC flux is required to properly explain the flux trends discussed above.

#### 4.2.1. POC export efficiency

Despite moderate NPP (according to Poulton et al., this issue) and a low contribution of fast-sinking particles to near-surface POC concentrations on the Agulhas Bank, we measured an extremely high export efficiency ratio (range: 0.58–9.26, Fig. 7a), with higher values inshore than offshore (median  $\pm$  SD:  $2.13 \pm 3.35$  and  $0.68 \pm 0.50$ , respectively). The ExEff measured here is not comparable to the previous studies which recorded the ExEff global ratio of  $\sim 0.18$  and the global modeled mean ratio of 0.22, as these studies were mostly conducted in the open ocean (Henson et al., 2015, 2019). ExEff is influenced by factors such as the phytoplankton community structure and microbial or zooplankton degradation of organic matter (Henson et al., 2011, 2012). For example, ExEff tends to be higher in regions where the phytoplankton community structure can produce large aggregates or sink by ballasting (Francois et al., 2002) or, alternatively, where there is an absence of grazers (Henson et al., 2015). In our study we expected to find lower ExEff on the Agulhas Bank than we observed, due to the nature of phytoplankton i.e., dominated by small-sized phytoplankton and low abundance of large Chl *a* aggregates.

Most of our stations with the highest ExEff ratios had low NPP (adopted from Poulton et al., this issue), suggesting a decoupling between NPP and ExEff which can be linked to a low abundance of grazers (Henson et al., 2019). For example, stations 11.1, 1.4, 10.2 and 9.1 had high ExEff but low-to-moderate NPP. Also, the POC sinking particles were dominated by fast-sinking particles in these stations, except for station 11.1 (Table S3). Unfortunately, we did not measure remineralization rates during the cruise to explain the high ExEff occurring simultaneously with low NPP, which was observed here. Similar scenarios of high ExEff coupled with low NPP are thought to be linked to ongoing POC export from a standing stock of biomass produced at the end of a previous bloom phase (Henson et al., 2015). For example, primary production requires time to convert particulate organic matter into sinking flux as it needs to reach a certain density to sink (Henson et al., 2015). This may lead to a mismatch between primary production and ExEff as the measured export flux might have been produced prior to the time of sampling. The observed high satellite-derived Chl *a* along the coastline before the cruise supports this argument (Figs. S5–S7). Therefore, it is likely that the high ExEff we observed here was derived from the primary production that occurred before the cruise. Although it is not possible to quantify this during *in situ* sampling, our explanation corresponds with the suggested post-upwelling scenario off Port Alfred (Giering et al., this issue).

#### 4.2.2. Transfer efficiency of POC, Chl *a* and bSi

Based on the particle structure observed in the study, we expected low transfer efficiencies in the AB because of the high suspended particle fraction. However, our POC, Chl *a* and bSi TE measurements were higher (range: 0.3–0.99, 0.15–1 and 0.2–33.04, respectively), suggesting that a large amount of exported organic carbon flux reached the bottom depths. These TEs are not comparable to global measurements due to the variability in reference depths. Most studies use a bottom reference depth of  $>500$  m (Francois et al., 2002; Henson et al., 2012) which is too deep to compare to our bottom reference depth of 100m. However, previous studies have suggested a spatial variation in TEs, with low latitudes having high TEs and high latitudes having low TEs (Francois et al., 2002; Klaas and Archer, 2002). This suggestion was based on the ecosystem structure (i.e., the high latitudes being dominated by opal and low latitudes dominated by carbonate) and on the ballasting effect

where the bottom carbonate fluxes were found to be correlated with TE, while opal flux showed no correlation (Francois et al., 2002; Klaas and Archer, 2002).

We noted that stations with low POC TEs had high ExEffs (for example, stations 1.4, 11.1 and 8.1). This trend can be explained by high microbial or zooplankton remineralization rates in the water column, resulting in the low transfer of organic carbon to the bottom. Stations 11.1 and 8.1 registered high zooplankton abundance and biovolume (Noyon et al., this issue), which is likely to contribute to organic carbon remineralization by releasing fecal pellets and thereby promoting bacterial remineralization of fecal pellets. Also, the vertical water column at station 11.1 contained low dissolved oxygen concentrations (Giering et al., this issue) and high nutrient concentrations at the bottom, suggesting a possibility of remineralization (Poulton et al., this issue). Therefore, it is highly likely that high remineralization was the factor associated with low TEs at stations 8.1 and 11.1.

Station 1.4 had low POC transfer efficiency (0.3) although it recorded large Chl-rich aggregates (Giering et al., this issue) in the upper 30 m and had high ExEff (6.5). Regions with the high abundance of large, fast-sinking aggregates are capable of having low transfer efficiency as aggregates decay rapidly as they sink (Lima et al., 2014). This scenario can explain the low transfer efficiency measured at station 1.4, as the Port Alfred area had been suggested to have large phytodetritus aggregates. However, our data was insufficient to conclude that remineralization was the factor here, leading to decaying phytoplankton aggregates. For example, the zooplankton abundance and biovolume was low, suggesting low grazing pressure by zooplankton on organic matter (Noyon et al., this issue). The pattern observed at station 1.4 differed from station 11.1 where there was low dissolved oxygen and a possibility of remineralization.

Station 10.2 had a high POC transfer efficiency (0.79) and high ExEff (2.2), suggesting low grazing pressure on the exported flux. Although bacterial abundance was not measured, zooplankton abundance and biovolume were low at station 10.2 (Noyon et al., this issue), suggesting low remineralization. According to García-Martín et al. (2021) and Henson et al. (2012), regions of low remineralization result in a high transfer of organic carbon to depth. Although station 10.2 also had high ExEff, the bottom MSC was close to the bottom ( $\sim 2.6$  m above the bottom, Table S1), improving the likelihood that the transfer efficiency was influenced by resuspended sediments (Lima et al., 2014). Based on the measured high POC ExEff and low zooplankton abundance, it is highly possible that transfer efficiency at station 10.2 was derived from exported POC flux, and likely influenced by resuspension.

We observed the highest POC transfer efficiency at station 5.5 (0.9), suggesting that most of exported organic carbon reached the bottom. This station had an intermediate surface diatom cell abundance of  $\sim 4000$  cells  $L^{-1}$  (Poulton et al., this issue), suggesting the vertical transport of POC to depth by dense aggregates. The presence of diatoms in the system can result in the ballasting of organic carbon with bSi which enhances the vertical transport of organic carbon to depth (Francois et al., 2002). We observed high bSi transfer efficiency on the Agulhas Bank, with station 5.5 recording the second highest transfer efficiency values (Fig. 8c). However, our data is insufficient to prove conclusively that sinking POC fraction was ballasted by bSi. In addition, although we expected to find similarities in the distribution pattern of POC and bSi to strengthen the ballasting hypothesis argument, this was not the case (Fig. 8a and c). Overall, spatial variability in our POC transfer efficiency values appeared to be explained by vertical export of organic matter, with an influence of sediment resuspension at station 10.2. It is unclear what caused high bSi TEs on the AB, however there is a possibility that bSi TEs were influenced by resuspended sediments as two of our three stations with the highest bSi TEs were sampled closer to the bottom depth, i.e., stations 9.1 and 10.2 (Table S1).

### 4.3. Particle fluxes as an implication for BNL formation

This section excludes the Port Alfred region due to its different biophysical dynamics. We observed a correlation between bottom turbidity (as a proxy for the benthic nepheloid layer) and export fluxes of POC, suggesting that POC export fluxes are associated with the formation of bottom turbidity (Fig. S2a). However, bSi export fluxes showed no correlation with the bottom turbidity, indicating that other factors such as sediment resuspension might have also influenced bottom turbidity (Figs. S2b and c). Although only POC export fluxes showed a significant positive correlation with the bottom turbidity ( $R^2 = 0.69$ ,  $p < 0.01$ ), Chl *a* export flux also showed a (non-significant) positive relationship with the bottom turbidity ( $R^2 = 0.31$ ,  $p = 0.06$ ), strengthening the possibility of BNL formation by export fluxes.

To support the link between bottom turbidity and export fluxes, we explored cross-shelf patterns of bottom turbidity on the Agulhas Bank. Our bottom turbidity showed a clear cross-shelf pattern, with inshore stations showing significantly higher turbidity than the offshore stations (Welch's *t*-test,  $p < 0.001$ , Fig. S3a), which corresponds to the cross-shelf pattern of POC fluxes (Mazwane et al. this study, this issue). Also, a timeseries of NPP satellite data confirms a cross-shelf pattern to support a strong link between exported phytodetritus and bottom turbidity, although the cross-shelf pattern of NPP was not significant during the cruise itself (Welch's *t*-test,  $p = 0.77$ , Fig. S3b). It is possible that the time lag in remineralization of exported phytodetritus (Giering et al., this issue) might have caused the absence of the link between cross-shelf distribution of surface NPP and bottom turbidity during the cruise. We therefore conclude that bottom turbidity (a proxy for BNL) and export POC fluxes were linked, keeping in mind that the resuspension of sediments might have also contributed to bottom turbidity where MSC sampling depths were close to the bottom.

### 4.4. Future work

Our data was inconclusive on certain observed trends. We suggest exploring factors such as microbial respiration rates and bacterial abundance; to quantify the bacterial contribution to remineralization throughout the water column. This would help to clarify the observed spatial patterns of fluxes, ExEff and transfer efficiency. Also, measuring other biomineral parameters such as  $\text{CaCO}_3$  would assist in formulating correlations with POC fluxes, as well as determining the ballast hypothesis. For example,  $\text{CaCO}_3$  is found in small-sized ( $<20 \mu\text{m}$ ) phytoplankton groups such as coccolithophores (Lima et al., 2014) and is known to ballast more with POC than biogenic silica (Francois et al., 2002). Although the Agulhas Bank was dominated by phytoplankton of  $<20 \mu\text{m}$ , we could not conclude that  $\text{CaCO}_3$  was able to ballast with carbon as this was beyond the scope of this study. As such, we suggest that quantifying particle material such as lithogenic or biogenic material and increasing the sample size would assist in making conclusive decisions about the composition of particles and fluxes on the Agulhas Bank.

## 5. Conclusion

We measured vertical carbon fluxes and investigated the spatial distribution of particle composition on the Agulhas Bank. Our data showed clear spatial variability, with inshore regions exhibiting higher fluxes than offshore stations. We observed a decoupling between POC, Chl *a* and bSi fluxes, i.e., POC and Chl *a* flux decreased with depth while bSi showed the opposite trend (Table S4). We conclude that vertical transport of organic matter and resuspension of sediments were the likely factors influencing the distribution of fluxes on the Agulhas Bank, primarily due to the shelf being shallow ( $<150 \text{ m}$ ). Our fluxes and particle composition were comparable to global studies. However, the export and transfer efficiencies were very high on the Agulhas Bank and not comparable to global studies as they were focused on the much

deeper open ocean. Higher transfer efficiencies are typically observed in regions influenced by phytoplankton bloom events (Francois et al., 2002), but the Agulhas Bank did not show any presence of an active bloom event during the cruise. We did suggest a possibility of bloom activity before the cruise based on satellite observations of surface Chl *a* and SST, which could have influenced the TEs. Our transfer efficiencies could have been influenced by the resuspension of bottom sediments in cases where the MSC sampled closer to the bottom, especially for bSi TEs which were very high compared to POC and Chl *a* TEs. We suggest that other unmeasured factors, such as the standing stock of carbon biomass and biomineral ballasting, might have influenced calculated fluxes during this cruise.

### Author contributions

**Nwabisa V. Malongweni:** Conceptualization, Investigation, Formal analysis, Writing – original draft, Writing – review & editing. **Emma Roche:** Conceptualization, Investigation, Writing – original draft, Writing – review & editing. **Mike Roberts:** Principal investigator, Funding acquisition. **Sarah L. C Giering:** Conceptualization, Investigation, Formal analysis, Writing – original draft, Writing – review & editing.

### Declaration of competing interest

The authors declare that they have no known competing financial interests or personal relationships that could have appeared to influence the work reported in this paper.

### Data availability

Data will be made available on request.

### Acknowledgements

We thank the Department of Forestry, Fisheries and Environmental Affairs (DFFE) crew for assistance during the research cruise. This publication was supported by the Global Challenges Research Fund (GCRF), UK, in the framework of the SOLSTICE-WIO project, NE/P021050/01. This work was also supported by the UK-SA Bilateral Chair of Ocean Science and Marine Food Security funded by the NRF - DST Grant (98399). We thank the South African Institute for Aquatic Biodiversity (SAIAB) - ACEP for funding. We thank the South African Observation Environmental Network for lab analysis platform. A special thanks to Hannah East, Tarryn Swartbooi, Mfundo Bizani and Patrick Vianello for laboratory and technical assistance.

### Appendix A. Supplementary data

Supplementary data to this article can be found online at <https://doi.org/10.1016/j.dsr2.2023.105334>.

### References

- Allredge, A.L., Silver, M.W., 1988. Characteristics, dynamics, and significance of marine snow. *Prog. Oceanogr.* 20, 41–82. [https://doi.org/10.1016/0079-6611\(88\)90053-5](https://doi.org/10.1016/0079-6611(88)90053-5).
- Armstrong, R.A., Lee, C., Hedges, J.I., Honjo, S., Wakeham, S.G., 2002. A new, mechanistic model for organic carbon fluxes in the ocean based on the quantitative association of POC with ballast minerals. *Deep Sea Res. Part II Top. Stud. Oceanogr.* 49, 219–236. [https://doi.org/10.1016/S0967-0645\(01\)00101-1](https://doi.org/10.1016/S0967-0645(01)00101-1).
- Atkinson, L.P., Yonder, J.A., Lee, T.N., 1984. Review of upwelling off the southeastern United States and its effect on continental-shelf nutrient concentrations and primary productivity. *Rapports et Procès-Verbaux des Réunions* 183, 70–78.
- Bach, L.T., Stange, P., Taucher, J., Achterberg, E.P., Algueró-Muniz, M., Horn, H., Esposito, M., Riebesell, U., 2019. The influence of plankton community structure on sinking velocity and remineralization rate of marine aggregates. *Global Biogeochem. Cycles* 33, 971–994. <https://doi.org/10.1029/2019GB006256>.
- Baker, C.A., Henson, S.A., Cavan, E.L., Giering, S.L., Yool, A., Gehlen, M., Belcher, A., Riley, J.S., Smith, H.E., Sanders, R., 2017. Slow-sinking particulate organic carbon in

- the Atlantic Ocean: magnitude, flux, and potential controls. *Global Biogeochem. Cycles* 31 (7), 1051–1065.
- Bakun, A., 1973. Coastal Upwelling Indices. west coast of North America, 1946–71.
- Banse, K., English, D.C., 2000. Geographical differences in seasonality of CZCS-derived phytoplankton pigment in the Arabian Sea for 1978–1986. *Deep Sea Res. Part II Top. Stud. Oceanogr.* 47 (7–8), 1623–1677.
- Beal, L.M., De Ruijter, W.P., Biastoch, A., Zahn, R., 2011. On the role of the Agulhas system in ocean circulation and climate. *Nature* 472 (7344), 429–436.
- Belcher, A., Iversen, M., Giering, S., Riou, V., Henson, S.A., Berline, L., Guilloux, L., Sanders, R., 2016. Depth-resolved particle-associated microbial respiration in the northeast Atlantic. *Biogeosciences* 13 (17), 4927–4943. <https://doi.org/10.5194/bg-13-4927-2016>.
- Biscaye, P.E., Eitrem, S.L., 1977. Suspended particulate loads and transports in the nepheloid layer of the abyssal Atlantic Ocean. *Mar. Geol.* 23 (1–2), 155–172.
- Boyd, A.J., Shillington, F.A., 1994. Physical forcing and circulation patterns on the Agulhas Bank. *South Afr. J. Sci.* 90 (3), 143–154.
- Boyd, A.J., Taunton-Clark, J., Oberholster, G.P.J., 1992. Spatial features of the near-surface and midwater circulation patterns off western and southern South Africa and their role in the life histories of various commercially fished species. *S. Afr. J. Mar. Sci.* 12 (1), 189–206.
- Boyd, P.W., Sundby, S., Pörtner, H.O., 2014. Cross-chapter box on net primary production in the ocean. In: *Climate Change 2014: Impacts, Adaptation, and Vulnerability. Part A: Global and Sectoral Aspects. Contribution of Working Group II to the Fifth Assessment Report of the Intergovernmental Panel of Climate Change.* Cambridge University Press, pp. 133–136.
- Brzezinski, M.A., 1985. The Si:C:N ratio of marine diatoms: interspecific variability and the effect of some environmental variables. *J. Phycol.* 21, 347–357. <https://doi.org/10.1111/j.0022-3646.198.00347.x>.
- Buesseler, K.O., Boyd, P.W., Black, E.E., Siegel, D.A., 2020. Metrics that matter for assessing the ocean biological carbon pump. *Proc. Natl. Acad. Sci. USA* 117 (18), 679–9687. <https://doi.org/10.1073/pnas.1918114117>.
- Buesseler, K.O., Ball, L., Andrews, J., Cochran, J.K., Hirschberg, D.J., Bacon, M.P., Fleer, A., Brzezinski, M., 2001. Upper ocean export of particulate organic carbon and biogenic silica in the Southern Ocean along 170° W. *Deep Sea Res. Part II Top. Stud. Oceanogr.* 48 (19–20), 4275–4297.
- Cavan, E.L., Trimmer, M., Shelley, F., Sanders, R., 2017. Remineralization of particulate organic carbon in an ocean oxygen minimum zone. *Nat. Commun.* 8 (1), 1–9. <https://doi.org/10.1038/ncomms14847>.
- Ceballos-Romero, E., Le Moigne, F.A., Henson, S., Marsay, C.M., Sanders, R.J., García-Tenorio, R., Villa-Alfageme, M., 2016. Influence of bloom dynamics on Particle Export Efficiency in the North Atlantic: a comparative study of radioanalytical techniques and sediment traps. *Mar. Chem.* 186, 198–210.
- Chen, A.T., Borges, A.V., 2009. Reconciling opposing views on carbon cycling in the coastal ocean: continental shelves as sinks and near-shore ecosystems as sources of atmospheric CO<sub>2</sub>. *Deep Sea Res. Part II Top. Stud. Oceanogr.* 56 (8–10), 578–590. <https://doi.org/10.1016/j.dsr2.2008.12.009>.
- de Haas, H., van Weering, T.C., de Stigter, H., 2002. Organic carbon in shelf seas: sinks or sources, processes and products. *Continent. Shelf Res.* 22 (5), 691–712.
- DeMaster, D.J., 1981. The supply and accumulation of silica in the marine environment. *Geochem. Cosmochim. Acta* 45 (10), 1715–1732.
- Dorfler, K.A., 2002. The Dynamics of Turbidity on the Spawning Grounds of Chokka Squid *Loligo Vulgaris* Reynaudii and Links to Squid Catches (MSc Dissertation). University of Port Elizabeth, South Africa.
- Ewing, M., Thorndike, E.M., 1965. Suspended matter in deep ocean water. *Science* 147 (3663), 1291–1294. <https://doi.org/10.1126/science.147.3663.1291>.
- Fan, H., Wang, X., Zhang, H., Yu, Z., 2018. Spatial and temporal variations of particulate organic carbon in the Yellow-Bohai Sea over 2002–2016. *Sci. Rep.* 8 (1), 1–9.
- Faugères, J.C., Mulder, T., 2011. Contour currents and contourite drifts. *Dev. Sedimentol.* 63, 149–214. <https://doi.org/10.1016/B978-0-444-53000-4.00003-2>.
- Fowler, S.W., Knauer, G.A., 1986. Role of large particles in the transport of elements and organic compounds through the oceanic water column. *Prog. Oceanogr.* 16, 147–194. [https://doi.org/10.1016/0079-6611\(86\)90032-7](https://doi.org/10.1016/0079-6611(86)90032-7).
- Francois, R., Honjo, S., Krishfield, R., Manganini, S., 2002. Factors controlling the flux of organic carbon to the bathypelagic zone of the ocean. *Global Biogeochem. Cycles* 16 (4). <https://doi.org/10.1029/2001GB001722>, 34–1.
- García-Martín, E.E., Davidson, K., Davis, C.E., Mahaffey, C., McNeill, S., Purdie, D.A., Robinson, C., 2021. Low contribution of the fast-sinking particle fraction to total plankton metabolism in a temperate shelf sea. *Global Biogeochem. Cycles* 35 (9), e2021GB007015.
- Gardner, W.D., Richardson, M.J., Mishonov, A.V., 2018. Global assessment of benthic nepheloid layers and linkage with upper ocean dynamics. *Earth Planet Sci. Lett.* 482, 126–134.
- Giering, S.L.C., Sanders, R.J., Martin, A.P., Lindemann, C., 2016. High export via small particles before the onset of the North Atlantic spring bloom. *J. Geophys. Res.: Oceans* 121 (9), 6929–6945.
- Giering, S.L., Noyon, M., Godfrey, B., Poulton, A.J., Carvalho, F. and Roberts, M., This issue. Optical particle measurements reveal cross-shelf turbidity gradients on the Agulhas Bank. *Deep Sea Res. Part II Top. Stud. Oceanogr.*, p.105094.
- Henson, S.A., Sanders, R., Madsen, E., 2012. Global patterns in efficiency of particulate organic carbon export and transfer to the deep ocean. *Global Biogeochem. Cycles* 26, 1–14. <https://doi.org/10.1029/2011GB004099>.
- Henson, S.A., Yool, A., Sanders, R., 2015. Global biogeochemical cycles carbon export: a model study. *Global Biogeochem. Cycles* 29, 33–45.
- Henson, S., Le Moigne, F., Giering, S., 2019. Drivers of carbon export efficiency in the global ocean. *Global Biogeochem. Cycles* 33 (7), 891–903.
- Henson, S.A., Sanders, R., Madsen, E., Morris, P.J., Le Moigne, F., Quartly, G.D., 2011. A reduced estimate of the strength of the ocean's biological carbon pump. *Geophys. Res. Lett.* 38 (4).
- Holt, J., Hyder, P., Ashworth, M., Harle, J., Hewitt, H.T., Liu, H., New, A.L., Pickles, S., Porter, A., Popova, E., Icarus Allen, J., Siddorn, J., Wood, R., 2017. Prospects for improving the representation of coastal and shelf seas in global ocean models. *Geosci. Model Dev. (GMD)* 10 (1), 499–523. <https://doi.org/10.5194/gmd-10-499-2017>.
- Hollister, C., McCave, I., 1984. Sedimentation under deep-sea storms. *Nature* 309, 220–225. <https://doi.org/10.1038/309220a0>.
- Hutchings, L., 1994. The Agulhas Bank: a synthesis of available information and a brief comparison with other east-coast shelf regions. *South Afr. J. Sci.* 90, 179–185.
- Hutchings, L., Beckley, L.E., Griffiths, M.H., Roberts, M.J., Sundby, S., van der Lingen, C., 2002. Spawning on the edge: spawning grounds and nursery areas around the southern African coastline. *Mar. Freshw. Res.* 53 (2), 307–318. <https://doi.org/10.1071/MF01147>.
- Isaki, K., Okamura, K., Kiyomoto, Y., 2003. Seasonality and composition of downward particulate fluxes at the continental shelf and Okinawa Trough in the East China Sea. *Deep Sea Res. Part II Top. Stud. Oceanogr.* 50, 457–473. [https://doi.org/10.1016/S0967-0645\(02\)00468-X](https://doi.org/10.1016/S0967-0645(02)00468-X).
- Kalle, K., 1937. Eine bemerkenswerte fluoreszenzerscheinung in wässriger diacytyllösung. *Naturwissenschaften* 25 (4), 61–61.
- Karp-Boss, L., Wheeler, P.A., Hales, B., Covert, P., 2004. Distributions and variability of particulate organic matter in a coastal upwelling system. *J. Geophys. Res.* 109 <https://doi.org/10.1029/2003JC002184>.
- Klaas, C., Archer, D.E., 2002. Association of sinking organic matter with various types of mineral ballast in the deep sea: implications for the rain ratio. *Global Biogeochem. Cycles* 16 (4). <https://doi.org/10.1029/2001gb001765>, 63–1.
- Krause, J.W., Schulz, I.K., Rowe, K.A., Dobbins, W., Winding, M.H., Sejr, M.K., Duarte, C. M., Agustí, S., 2019. Silicic acid limitation drives bloom termination and potential carbon sequestration in an Arctic bloom. *Sci. Rep.* 9 (1), 1–11.
- Kudo, I., Yoshimura, T., Yanada, M., Matsunaga, K., 2000. Exhaustion of nitrate terminates a phytoplankton bloom in Funka Bay, Japan: change in SiO<sub>4</sub>:NO<sub>3</sub> consumption rate during the bloom. *Mar. Ecol. Prog. Ser.* 193, 45–51. <https://doi.org/10.3354/meps193045>.
- Largier, J.L., Swart, V.P., 1987. East-west variation in thermocline breakdown on the Agulhas Bank. *S. Afr. J. Mar. Sci.* 5 (1), 263–272. <https://doi.org/10.2989/025776187784522252>.
- Lee, C., Murray, D.W., Barber, R.T., Buesseler, K.O., Dymond, J., Hedges, J.I., Honjo, S., Manganini, S.J., Marra, J., Moser, C., Peterson, M.L., Prell, W.L., Wakeham, S.G., 1998. Particulate organic carbon fluxes: compilation of results from the 1995 US JGOFS Arabian Sea process study. *Deep Sea Res. Part II Top. Stud. Oceanogr.* 45, 2489–2501. [https://doi.org/10.1016/S0967-0645\(98\)00079-4](https://doi.org/10.1016/S0967-0645(98)00079-4).
- Le Moigne, F.A., Henson, S.A., Sanders, R.J., Madsen, E., 2013. Global database of surface ocean particulate organic carbon export fluxes diagnosed from the 234 Th technique. *Earth Syst. Sci. Data* 5 (2), 295–304.
- Leynaert, A., Tréguer, P., Queguiner, B., Morvan, J., 1991. The distribution of biogenic silica and the composition of particulate organic matter in the Weddell-Scotia Sea during spring 1988. *Mar. Chem.* 35 (1–4), 435–447.
- Lima, I.D., Lam, P.J., Doney, S.C., 2014. Dynamics of particulate organic carbon flux in a global ocean model. *Biogeosciences* 11 (4), 1177–1198.
- Lipiński, M.R., van der Vyver, J.S.F., Shaw, P., Sauer, W.H.H., 2016. Life cycle of chokka squid *Loligo reynaudii* in South African waters. *Afr. J. Mar. Sci.* 38, 589–593. <https://doi.org/10.2989/1814232X.2016.1230074>.
- Liu, K.K., Atkinson, L., Chen, C.T.A., Gao, S., Hall, J., Macdonald, R.W., McManus, L.T., Quinones, R., 2000. Exploring continental margin carbon fluxes on a global scale. *Eos, Transactions American Geophysical Union* 81 (52), 641–644.
- Longhurst, A., Sathyendranath, S., Platt, T., Caverhill, C., 1995. An estimate of global primary production in the ocean from satellite radiometer data. *J. Plankton Res.* 17, 1245–1271. <https://doi.org/10.1093/plankt/17.6.1245>.
- Lutjeharms, J.R.E., 2006. *The Agulhas Current*. Springer, Germany.
- Lutjeharms, J.R.E., Cooper, J., Roberts, M., 2000. Upwelling at the inshore edge of the agulhas current. *Continent. Shelf Res.* 20 (7), 737–761.
- Lutz, M., Dunbar, R., Caldeira, K., 2002. Regional variability in the vertical flux of particulate organic carbon in the ocean interior. *Global Biogeochem. Cycles* 16 (3), 11–1.
- Martin, J.H., Knauer, G.A., Karl, D.M., Broenkow, W.W., 1987. VERTEX: carbon cycling in the northeast Pacific. *Deep Sea Research Part A. Oceanographic Res. Papers* 34 (2), 267–285.
- Mazwane, S.L., Poulton, A.J., Hickman, A.E., Jebri, F., Jacobs, Z., Roberts, M. and Noyon, M., This issue. Spatial and temporal variability of net primary production on the Agulhas Bank, 1998–2018. *Deep Sea Res. Part II Top. Stud. Oceanogr.*, p.105079.
- McCave, I.N., 1983. Particulate size spectra, behavior, and origin of nepheloid layers over the Nova Scotian continental rise. *J. Geophys. Res.: Oceans* 88 (C12), 7647–7666. <https://doi.org/10.1029/JC088iC12p07647>.
- McCave, I.N., Hall, I.R., 2002. Turbidity of waters over the Northwest Iberian continental margin. *Prog. Oceanogr.* 52 (2–4), 299–313.
- Middelburg, J.J., 2019. *Marine carbon biogeochemistry: a primer for earth system scientists - primary production: from inorganic to organic carbon*. Springer Briefs in Earth System Sciences. Nature 118.
- Millan-Núñez, R., Alvarez-Borrego, S., Nelson, D.M., 1982. Effects of physical phenomena on the distribution of nutrients and phytoplankton productivity in a coastal lagoon. *Estuar. Coast Shelf Sci.* 15, 317–335. [https://doi.org/10.1016/0272-7714\(82\)90066-X](https://doi.org/10.1016/0272-7714(82)90066-X).

- Mortlock, R.A., Froelich, P.N., 1989. A simple method for the rapid determination of biogenic opal in pelagic marine sediments. *Deep Sea Research Part A. Oceanographic Res. Papers* 36, 1415–1426. [https://doi.org/10.1016/0198-0149\(89\)90092-7](https://doi.org/10.1016/0198-0149(89)90092-7).
- Muller-Karger, F., Varela, R., Thunell, R., Astor, Y., Zhang, H., Luerssen, R., Hu, C., 2004. Processes of coastal upwelling and carbon flux in the Cariaco Basin. *Deep Sea Res. Part II Top. Stud. Oceanogr.* 51, 927–943. <https://doi.org/10.1016/j.dsr2.2003.10.010>.
- Noyon, M., 2019. Ellen Khuzwayo EK188 – cruise summary report. Southampton 61. [https://www.bodc.ac.uk/resources/inventories/cruise\\_inventory/reports/ellenkhuzwayo\\_188.pdf](https://www.bodc.ac.uk/resources/inventories/cruise_inventory/reports/ellenkhuzwayo_188.pdf).
- Noyon, M., Poulton, A.J., Asdar, S., Weitz, R. and Giering, S.L., This issue. Mesozooplankton community distribution on the Agulhas Bank in autumn: size structure and production. *Deep Sea Res. Part II Top. Stud. Oceanogr.*, 195, p.105015.
- Omand, M.M., Govindarajan, R., He, J., Mahadevan, A., 2020. Sinking flux of particulate organic matter in the oceans: sensitivity to particle characteristics. *Sci. Rep.* 10 (1), 1–16.
- Pak, H., Zaneveld, J.R.V., 1977. Bottom nepheloid layers and bottom mixed layers observed on the continental shelf of Oregon. *J. Geophys. Res.* 82 (27), 3921–3931.
- Poulton, A.J., Mazwane, S.L., Godfrey, B., Carvalho, F., Mawji, E., Wihsgott, J.U. and Noyon, M., This issue. Primary production dynamics on the Agulhas Bank in autumn. *Deep Sea Res. Part II Top. Stud. Oceanogr.*
- Probyn, T., Mitchell-Innes, B., Brown, P., Hutchings, L., Carter, R., 1994. A review of primary production and related processes on the Agulhas Bank. *South Afr. J. Sci.* 90 (3), 166–173.
- Ragueneau, O., Tréguer, P., 1994. Determination of biogenic silica in coastal waters: applicability and limits of the alkaline digestion method. *Mar. Chem.* 45 (1), 43–51. [https://doi.org/10.1016/0304-4203\(94\)90090-6](https://doi.org/10.1016/0304-4203(94)90090-6).
- Ragueneau, O., Schultes, S., Bidle, K., Claquin, P., Moriceau, B., 2006. Si and C interactions in the world ocean: importance of ecological processes and implications for the role of diatoms in the biological pump. *Global Biogeochem. Cycles* 20 (4). <https://doi.org/10.1029/2006GB002688>.
- R Core Team, 2019. R: A Language and Environment for Statistical Computing. R Foundation for Statistical Computing, Vienna, Austria. <https://www.R-project.org/>.
- Reigstad, M., Wexels, C., Wassmann, P., Ratkova, T., 2008. Vertical export of particulate organic carbon: attenuation, composition and loss rates in the northern Barents Sea. *Deep-Sea Research II* 55, 2308–2319. <https://doi.org/10.1016/j.dsr2.2008.05.007>.
- Riley, J.S., Sanders, R., Marsay, C., Le Moigne, F.A., Achterberg, E.P., Poulton, A.J., 2012. The relative contribution of fast and slow sinking particles to ocean carbon export. *Global Biogeochem. Cycles* 26 (1), p10.
- Roberts, M.J., Sauer, W.H.H., 1994. Environment: the key to understanding the South African chokka squid (*Loligo vulgaris reynaudii*) life cycle and fishery? *Antarct. Sci.* 6 (2), 249–258. <https://doi.org/10.1017/S0954102094000386>.
- Roberts, M.J., van den Berg, M., 2005. Currents along the Tsitsikamma coast SA and potential transport of squid paralarvae-ichthyoplankton. *Afr. J. Mar. Sci.* 27 (2), 375–388.
- Roberts, M.J., Popova, E., Sauer, W.H.H. and Carter, L., This issue. The SOLSTICE SA project: dynamics of the Agulhas Bank, ecosystem functioning, regime shifts, catch crashes and future trends in the South African squid fishery. *Deep Sea Res. Part II Top. Stud. Oceanogr.*
- Schumann, E.H., Beekman, L.J., 1984. Ocean temperature structures on the Agulhas Bank. *Trans. Roy. Soc. S. Afr.* 45 (2), 191–203. <https://doi.org/10.1080/00359198409519483>.
- Shideler, G.L., 1981. Regional setting the South Texas shelf study area within the western Gulf of Mexico begins. *Mar. Geol.* 41 (1–2), 37–61.
- Shin, J.W., Park, J., Choi, J.G., Jo, Y.H., Kang, J.J., Joo, H.T., Lee, S.H., 2017. Variability of phytoplankton size structure in response to changes in coastal upwelling intensity in the southwestern east sea. *J. Geophys. Res.* 122, 10262–10274. <https://doi.org/10.1002/2017JC013467>.
- Simpson, J.H., Sharples, J., 2012. *Introduction to the Physical and Biological Oceanography of Shelf Seas*. Cambridge University Press.
- Subhas, A.V., Pavia, F.J., Dong, S., Lam, P.J., 2023. Global trends in the distribution of biogenic minerals in the Ocean. *J. Geophys. Res.*: Oceans 128 (2), e2022JC019470. <https://doi.org/10.1029/2022JC019470>.
- Swart, V.P., Largier, J.L., 1987. Thermal structure of Agulhas bank water. *S. Afr. J. Mar. Sci.* 5, 243–252. <https://doi.org/10.2989/025776187784522153>, 799.
- Taucher, J., Stange, P., Algueró-Muñiz, M., Bach, L.T., Nauendorf, A., Kolzenburg, R., Büdenbender, J., Riebesell, U., 2018. In situ camera observations reveal major role of zooplankton in modulating marine snow formation during an upwelling-induced plankton bloom. *Prog. Oceanogr.* 164, 75–88.
- Thomas, H., Bozec, Y., Elkalay, K., De Baar, H.J.W., 2004. Enhanced open ocean storage of CO<sub>2</sub> from shelf sea pumping. *Science* 304 (5673), 1005–1008. <https://doi.org/10.1126/science.1095491>.
- Townsend, D.W., Mayer, L.M., Dortch, Q., Spinrad, R.W., 1992. Vertical structure and biological activity in the bottom nepheloid layer of the Gulf of Maine. *Continent. Shelf Res.* 12, 367–387. [https://doi.org/10.1016/0278-4343\(92\)90037-K](https://doi.org/10.1016/0278-4343(92)90037-K).
- Turner, J.T., 2002. Zooplankton fecal pellets, marine snow and sinking phytoplankton blooms. *Aquat. Microb. Ecol.* 27 (1), 57–102.
- Turner, J.T., 2015. Zooplankton fecal pellets, marine snow, phytodetritus and the ocean's biological pump. *Prog. Oceanogr.* 130, 205–248.
- Walker, N.D., 1986. Satellite observations of the agulhas current and episodic upwelling south of Africa. *Deep Sea Research Part A. Oceanographic Res. Papers* 33 (8), 1083–1106.
- Watson, R., Pauly, D., 2001. Systematic distortions in world fisheries catch trends. *Nature* 414, 534–536. <https://doi.org/10.1038/35107050>.
- Welschmeyer, N.A., 1994. Fluorometric analysis of chlorophyll-a in the presence of chlorophyll-b and 861 phaeopigments. *Limnol. Oceanogr.* 39 (8), 1985–1992.
- Yokomizo, H., Botsford, L.W., Holland, M.D., Lawrence, C.A., Hastings, A., 2010. Optimal wind patterns for biological production in shelf ecosystems driven by coastal upwelling. *Theor. Ecol.* 3, 53–63. <https://doi.org/10.1007/s12080-009-0053-5>.
- Zoutendyk, P., 1972. The biology of the Agulhas sole, *Austroglossus pectoralis*, Part 1. Environment and trawling grounds. *Trans. Roy. Soc. S. Afr.* 40 (5), 349–366. <http://10.1080/00359197209519429>.
- Zoutendyk, P., Duvenage, I.R., 1989. Composition and biological implications of a nepheloid layer over the inner agulhas bank near mossel bay, South Africa. *Trans. Roy. Soc. S. Afr.* 47, 187–197. <https://doi.org/10.1080/00359198909520162>.